Model solution for volume reflection of relativistic particles in a bent crystal

M. V. Bondarenco*

Kharkov Institute of Physics and Technology, 1 Academic St., 61108 Kharkov, Ukraine

(Received 20 May 2010; published 29 October 2010)

For volume reflection process in a bent crystal, exact analytic expressions for positively- and negatively-charged particle trajectories are obtained within a model of parabolic continuous potential in each interplanar interval, with the neglect of incoherent multiple scattering. In the limit of the crystal bending radius greatly exceeding the critical value, asymptotic formulas are obtained for the particle mean deflection angle in units of Lindhard's critical angle, and for the final beam profile. Volume reflection of negatively charged particles is shown to contain effects of rainbow scattering and orbiting, whereas with positively charged particles none of these effects arise within the given model. The model predictions are compared with experimental results and numerical simulations. Estimates of the volume reflection mean angle and the final beam profile robustness under multiple scattering are performed.

DOI: 10.1103/PhysRevA.82.042902 PACS number(s): 61.85.+p, 29.27.−a, 45.10.−b

I. INTRODUCTION

The volume reflection is an effect of deflection of high-energy charged particles upon their *over-barrier* (nonchanneled) passage through a planarly oriented bent crystal. The effect arises when the crystal bending radius R greatly exceeds the critical value R_c. That condition is the same as the Tsyganov's one for the possibility of channeling in a bent crystal [1], but the particle motion regime in the crystal yet depends on the particle entry angle relative to the active atomic planes. When this angle is much larger than the critical value θ_c, then, moving in the continuous potential of bent planes, conserving the particle full transverse (radial) energy, the particles are rarely captured into channels (via incoherent scattering on atomic electrons and nuclei), and are mostly deflected elastically through the volume reflection mechanism. Curiously, the latter deflection proceeds to the side *opposite* to that of the crystal bending; the value of the deflection angle is of the order of critical angle θ_c. Furthermore, the particle beam after deflection remains fairly well collimated, i.e., its angular dispersion keeps much smaller than the mean deflection angle. That phenomenon was discovered in numerical simulations two decades ago [2] and recently verified experimentally [3,4]. Nowadays it is considered to be an option for beam collimation and partial extraction at ultrarelativistic charged-particle accelerators [5–7].

To a good accuracy, the particle dynamics in the volume reflection problem is classical [8] and reduces to classical particle motion in a cylindrically symmetrical continuous potential of bent atomic planes. Therewith, granted the angular momentum conservation relative to the active crystallographic plane bending axis, the final deflection angle is expressible in the standard way as an integral over the radial coordinate from an inverse square root function involving the potential [see Eq. (55b) below]. That representation served as a starting point for a number of numerical studies [2,9].

Although the computational problem as described above seems to be sufficiently simple, it is aggravated by the presence of several parameters: the ratio R/R_c, initial and final particle variables (impact parameter and the angles of incidence and deflection). The dependencies on all those parameters involve singularities, which in general are better dealt with by analytic techniques than by numerical ones. Besides that, as long as for practice mostly interesting is the case $R \gg R_c$, it would be instructive to evaluate the asymptotic behavior of all relevant observables in the formal limit $R/R_c \to \infty$, including next-to-leading-order corrections in the small parameter R_c/R. But since volume reflection depends on the particle dynamics in not one but the whole sequence of interplanar intervals, for feasibility of its global analytic description one rather needs a simplified model.

A valuable opportunity for realistic model building is that the interplanar potential in a silicon crystal, at least in the orientation (110), is fairly close to parabolic shape over the *entire* interplanar interval (see, e.g., [10]). A parabolic (harmonic) potential, i.e., a linear oscillator, permits a simple solution for the particle trajectory within a single interplanar interval. The next problem is to connect solutions on the boundaries of the adjacent intervals. It may appear nontrivial, but it is feasible to do that transitively, i.e., simultaneously for an arbitrary number of the adjacent intervals. Thereby we obtain a completely solvable model capturing basic features of the volume reflection, except the effects of incoherent multiple scattering. Moreover, we are able to derive not only the deflection angle, but also an expression for the whole trajectory, which further on may be used for description of inelastic processes, such as volume capture or electromagnetic radiation.

In the present work, we will deliver a solution for the suggested model problem. The plan of the article is as follows. In Sec. II we describe the procedure for connection of solutions between adjacent interplanar intervals, demonstrating that the problem reduces to elementary trigonometry. The particle trajectory is expressed as an explicit function of interplanar interval order number (not in terms of a recursive procedure), for an arbitrary ratio R/R_c. In Sec. III, from the obtained solution for the trajectory, we derive the particle final deflection angle, in form of a sum of inverse trigonometric (for positively charged particles) or hyperbolic (for negatively charged particles) functions. In Sec. IV we scrutinize the limit $R \gg R_c$, important for practical applications of volume reflection, first for positively, then for negatively charged particles. In the

*bon@kipt.kharkov.ua

generic expression for the final deflection angle, we find a possibility to replace the sums involved by integrals (via the Euler-Maclaurin formula), and do the latter ones in a closed form. As a result, we arrive at sufficiently simple asymptotic formulas for the deflection angle dependence on all the variables. The impact parameters are thereupon analytically averaged over, and the experimentally observable scattering differential cross section is obtained for positive and negative particles. In Sec. V we examine the opposite limit, $R \ll R_c$. In Sec. VI we provide estimates of optimal crystal and initial beam parameters for beam complete deflection or for experimental investigation of the final beam profile features. A summary is given in Sec. VII.

II. PARTICLE TRAJECTORY IN A BENT CRYSTAL

A. Initial conditions

The usual geometry of experiments on volume reflection implies a low-divergence charged-particle beam impact normally to a thin,[1] weakly bent single-crystal plate. The practically unavoidable slight curvature of the crystal boundary is of minor consequence, since the main contribution to the particle reflection angle comes from the vicinity of some point in the depth of the crystal. For definiteness and to establish an easy connection with the particle impact parameter in the initial (perfectly parallel[2]) beam, let us consider a particle incident along the z axis on a crystal whose front face is a *perfect plane*, located at $z = 0$. As for the crystal rear face, for our purposes in this paper we may leave it unspecified, as if the crystal was infinitely thick but transparent. Then, let θ_0 $(0 < \theta_0 \ll 1)$ be the angle of inclination of the crystalline planes to the z axis at the crystal front face (see Fig. 1), and let the x axis, perpendicular to Oz, point in the direction of the crystal bend. Moving at small angles to the crystal planes, the particle interacts most strongly (coherently) with the averaged, so-called continuous interplanar potential [8], which induces a force with a dominant x component (yet slowly dependent on z).[3] Along the y coordinate there is a translational invariance, ensuring conservation of the particle momentum y-component.

In single crystals of not too heavy chemical elements, in particular for silicon (diamond-type lattice), oriented by its (110) plane close to the direction of the beam, the continuous potential in each interplanar interval may closely be approximated by a quadratic function, with an accuracy of $\lesssim$20%.[4] That entails a linear equation of motion for the classical[5] ultrarelativistic[6] particle:

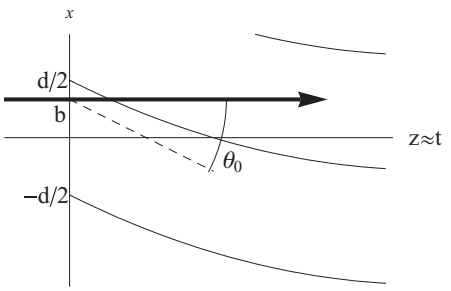

FIG. 1. Coordinates describing the bent crystal geometry (circle segments are the bent atomic planes) and the particle entrance to the crystal (thick arrow). Not to scale. For details see text.

$$\ddot{x} = \frac{2F_{\max}}{Ed}\,(-x + x_0)\,, \tag{1}$$

$$t \approx z \quad (c = 1, \quad \text{small angle motion}), \tag{2}$$

where x_0 is the midpoint of the interplanar interval, d the interplanar distance, E the particle energy, and $F_{\max}$ the force acting on the particle at the edge of the interplanar interval $x - x_0 = -\frac{d}{2}$. For positively charged particles, $F_{\max}$ is positive, whereas for negatively charged particles it is negative. Note that the force and the particle energy enter Eq. (1) only through the ratio

$$\frac{E}{|F_{\max}|} = R_c, \tag{3}$$

known as the Tsyganov critical radius [1]. The natural time unit in channeling-related phenomena is

$$\tau = \sqrt{\frac{Ed}{2|F_{\max}|}} \equiv \sqrt{\frac{R_c d}{2}} \tag{4}$$

($2\pi\tau$ has the meaning of a positively charged particle channeling period, although herein we deal with over-barrier motion, not with channeling).

Next, the crystal bending has the only consequence that x_0 in Eq. (1) acquires a dependence on the longitudinal coordinate

[1]The crystal has to be thin to avoid accumulation of incoherent multiple scattering effects, but still it may be thick enough for the volume reflection to occur within the crystal volume and be independent of the boundaries. We shall quantify the corresponding conditions later on (Sec. VI).

[2]We can turn to the issue of the initial beam divergence after we derive the scattering differential cross section.

[3]At the crystal boundary, z component of the force is not small compared to its x component, but the edge effects must certainly be negligible for a deeply penetrating particle. The boundary condition will be determined more precisely below.

[4]The condition thereof is that Thomas-Fermi radius of lattice-forming atoms be commensurable with the interatomic distance half width. In silicon, that is the case we have. As for crystals of heavier elements such as tungsten, there the atomic radius is appreciably smaller, and the parabolic approximation for the interplanar continuous potential is poor.

[5]It is standard [8] that, for a high-energy particle interacting with an oriented crystal, the particle wavelength shortness on the atomic scale makes the particle dynamics essentially classical, but yet nonperturbative, given the small angle of particle motion relative to a crystallographic direction and thus coherent action of atomic forces over long distances. Still, quantum effects may be viable in a special case when the particle transverse energy is very close to the height of an atomic potential barrier (the author is indebted to A.V. Shchagin for pointing this out in private conversation), but in any case, the classical calculation has to pave the way.

[6]Equation (1) in itself may apply to a nonultrarelativistic motion, too, provided E includes the particle rest energy (whereby, in the nonrelativistic limit $E \to m$). But physically, to not complicate the analysis, we confine ourselves in the present paper to the (experimentally most important) ultra-relativistic case.

z, which for ultrarelativistic motion under small angles to Oz may be equated to the current time t:

$$x_0 = x_0(z \approx t) \quad \text{(the crystal bend function)}. \tag{5}$$

In application to volume reflection, we are interested in a uniform bending of the crystal, at which $x_0(t)$ describes a circular arc of a small opening angle. That small arc may equally well be approximated by a parabola, and hence $x_0(t)$ is determined by the equation

$$x_0(t) = -\theta_0 t + \frac{t^2}{2R} \quad \text{(uniformly bent crystal)}, \tag{6}$$

where R is the atomic plane bending radius [without the loss of generality, one may let $x_0(0) = 0$; see Fig. 1].

Inserting (6) into (1), and implementing (4), we obtain the particle equation of motion in the first interplanar interval:

$$\ddot{x} = \pm\frac{1}{\tau^2}\left(-x - \theta_0 t + \frac{t^2}{2R}\right) \quad \begin{Bmatrix}\text{pos. charged particles}\\ \text{neg. charged particles}\end{Bmatrix}. \tag{7}$$

Initial conditions for $x(t)$ stand as

$$x(0) = b, \tag{8}$$

$$\dot{x}(0) = 0, \tag{9}$$

where b, restricted to the interval

$$-\frac{d}{2} \leqslant b \leqslant \frac{d}{2}, \tag{10}$$

is the impact parameter measured from the interval midpoint.[7] The equations of motion further simplify in terms of the "subtracted radius" variable

$$r(t) = -x(t) - \theta_0 t + \frac{t^2}{2R}, \tag{11}$$

becoming

$$\ddot{r} = \frac{\delta \mp r}{\tau^2} \quad \left(\text{in} -\frac{d}{2} \leqslant r \leqslant \frac{d}{2}\right), \tag{12}$$

where

$$\delta = \frac{\tau^2}{R}. \tag{13}$$

Thus, $\pm\delta$ is the spatial shift of the oscillator equilibrium position due to the crystal bend, i.e., due to the centrifugal force, which in the present small-angle approximation, presuming condition $r \ll R$ within the weakly bent crystal, is treated as virtually independent of the subtracted radius r (cf. [2]). For $r(t)$, the initial conditions (8) and (9) translate to

$$r(0) = -b, \tag{14}$$

$$\dot{r}(0) = -\theta_0. \tag{15}$$

Generic solution of Eq. (12) reads:

$$r_0(t) = \pm\delta - A_0 \begin{Bmatrix}\sin\\ \sinh\end{Bmatrix}\left(\frac{t}{\tau} + \varphi_0\right). \tag{16}$$

(Here and henceforth upper signs and figures refer to positively charged particles, and lower ones to negatively charged particles.) Matching initial conditions (14) and (15) allows one to determine the constants A_0 and φ_0:

$$A_0 = \sqrt{\tau^2\theta_0^2 \pm (b \pm \delta)^2}, \tag{17}$$

$$\varphi_0 = \begin{Bmatrix}\arcsin\\ \operatorname{arsinh}\end{Bmatrix}\frac{b \pm \delta}{A_0}. \tag{18}$$

[The sign of A_0 must be chosen positive so that $\dot{r}(0)$ at $\theta_0 > 0$, according to (15), is negative.]

Further on, solution (16) is to be connected with solutions in the subsequent interplanar intervals. Importantly, since the connection is to be carried out at definite r, the condition of the connection will not depend on the current phase of the harmonic motion, such as φ_0 in Eq. (16), as we are going to show.

B. Connection of solutions through interval borders

Moving along trajectory (16), the particle will cross the next interplanar interval border $r = -\frac{d}{2}$ at an instant

$$\frac{t_1}{\tau} = \begin{Bmatrix}\arcsin\\ \operatorname{arsinh}\end{Bmatrix}\frac{\frac{d}{2} \pm \delta}{A_0} - \varphi_0, \tag{19}$$

which is inferred from (16) by letting $r = -\frac{d}{2}$ and solving for t. At this instant, the equation of the particle motion turns to

$$\ddot{r} = \frac{\delta \mp (d + r)}{\tau^2} \quad \left(\text{in} -\frac{3d}{2} \leqslant r \leqslant -\frac{d}{2}\right). \tag{20}$$

That is again the same harmonic oscillator, only with an altered equilibrium position, so the general solution of (20) may be written

$$r_1(t) = \pm\delta - d - A_1 \begin{Bmatrix}\sin\\ \sinh\end{Bmatrix}\left(\frac{t}{\tau} + \varphi_0 + \Delta\varphi_1\right). \tag{21}$$

Values of new constants A_1, $\Delta\varphi_1$ are now to be determined from the continuity of $r(t)$ and $\dot{r}(t)$ at the interval border point $r = -\frac{d}{2}$. That can be done without formally solving the system of two equations. First, compare two integrals of motion

$$A_1^2 = \tau^2\dot{r}_1^2 \pm (\pm\delta - d - r_1)^2, \tag{22}$$

$$A_0^2 = \tau^2\dot{r}_0^2 \pm (\pm\delta - r_0)^2 \tag{23}$$

(related to transverse energy, see Eq. (57) below) in their common point, where $r_0 = r_1 = -\frac{d}{2}, \dot{r}_0 = \dot{r}_1$. Subtracting (23) from (22), one gets $A_1^2 = A_0^2 - 2\delta d$, i.e.,

$$A_1 = \sqrt{A_0^2 - 2\delta d}. \tag{24}$$

[7] Equation (9), holding exactly inside as well as outside of the crystal, deserves a comment. It implies the absence of refraction on the crystal boundary, although there is a b dependent jump in the potential energy (assuming that the particle enters the crystal about normally to its boundary and to the corresponding potential wall). The jump in the potential must also entail the opposite change in the particle kinetic energy, but it is very small compared to the beam energy (and its uncertainty even), anyway. Examination of our final results also proves that possible b dependence of the particle intra-crystal total energy can be safely neglected within the adopted accuracy. Note that b dependence of the initial (potential) energy will lead to extra sensitivity of the final deflection angle to the impact parameter (see Fig. 4 below), though it will have no effect on the appropriately averaged differential cross section.

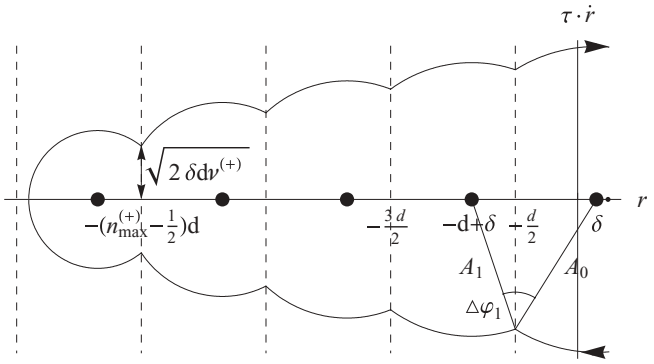

FIG. 2. Solid curve shows the phase-space (the subtracted radius r vs the radial velocity $\dot{r}$) trajectory for positively charged particles, under condition $\delta < \frac{d}{2}$. Dashed vertical lines signify the positions of the bent atomic planes (definite r). Thick dots indicate centers of the trajectory circular segments. Vertex angle $\Delta\varphi_1$ (and similarly all other $\Delta\varphi_n$) may be interpreted as a geometric sum of vertex angles in a pair of right triangles having a common cathetus, and with the second catheti equal $\frac{d}{2}+\delta$, $\frac{d}{2}-\delta$, and the hypotenuses A_0, A_1.

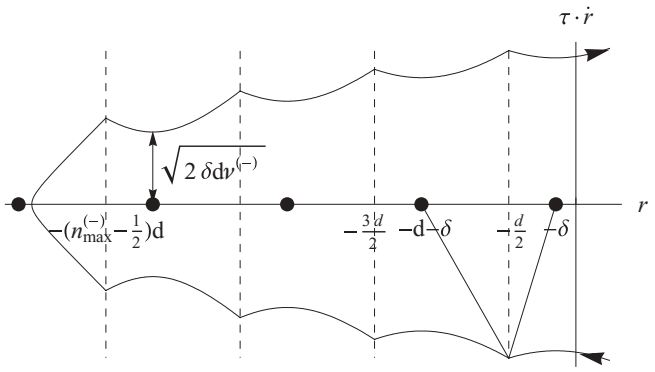

FIG. 3. Same as Fig. 2, but for negatively charged particles, assuming condition $\delta < \frac{d}{2}$ (see Sec. III B).

Thereupon, the phase shift $\Delta\varphi_1$ is sought from the condition $r_1(t_1) = -\frac{d}{2}$. One finds:

$$\Delta\varphi_1 = -\begin{Bmatrix}\arcsin\\ \operatorname{arsinh}\end{Bmatrix}\frac{\frac{d}{2}\pm\delta}{A_0} - \begin{Bmatrix}\arcsin\\ \operatorname{arsinh}\end{Bmatrix}\frac{\frac{d}{2}\mp\delta}{A_1} \tag{25}$$

(for a geometric interpretation of this relation for positive particles, see Fig. 2). As we had expected, neither A_1 nor $\Delta\varphi_1$ depends on φ_0.

At each subsequent border, the connection of the solutions is carried out in exactly the same way. Writing in the nth interval

$$r_n(t) = \pm\delta - nd - A_n\begin{Bmatrix}\sin\\ \sinh\end{Bmatrix}\left(\frac{t}{\tau}+\varphi_0+\sum_{m=1}^{n}\Delta\varphi_m\right),$$
$$-\frac{d}{2} - nd \leqslant r_n \leqslant \frac{d}{2} - nd, \quad t_n \leqslant t \leqslant t_{n+1}, \tag{26}$$

the generic amplitude is found as

$$A_n = \sqrt{A_{n-1}^2 - 2\delta d} = \sqrt{A_0^2 - 2n\delta d}$$
$$= \sqrt{\tau^2\theta_0^2 \pm (b\pm\delta)^2 - 2n\delta d}, \tag{27}$$

and the generic phase shift is deduced to be

$$\Delta\varphi_n = -\begin{Bmatrix}\arcsin\\ \operatorname{arsinh}\end{Bmatrix}\frac{\frac{d}{2}\pm\delta}{A_{n-1}} - \begin{Bmatrix}\arcsin\\ \operatorname{arsinh}\end{Bmatrix}\frac{\frac{d}{2}\mp\delta}{A_n}, \tag{28}$$

where the amplitudes in the denominators must be treated as already known, by (27). The instants of border passage can also be evaluated:

$$\frac{t_n}{\tau} = \sum_{m=1}^{n}\begin{Bmatrix}\arcsin\\ \operatorname{arsinh}\end{Bmatrix}\frac{\frac{d}{2}\pm\delta}{A_{m-1}} + \sum_{m=1}^{n-1}\begin{Bmatrix}\arcsin\\ \operatorname{arsinh}\end{Bmatrix}\frac{\frac{d}{2}\mp\delta}{A_m}$$
$$-\begin{Bmatrix}\arcsin\\ \operatorname{arsinh}\end{Bmatrix}\frac{b\pm\delta}{A_0} \qquad (r_{n-1}\to r_n). \tag{29}$$

One caution is that amplitudes A_n should not be regarded as a measure of the particle spatial wiggling in each interval. As Figs. 2 and 3 indicate, the trajectory swinging *enhances* as the particle penetrates deeper into the crystal, whereas amplitudes A_n, to the contrary, *decrease*. There is no contradiction here because for most of the intervals traversed, the intrachannel oscillation period $2\pi\tau$ is much greater than the time of particle passage across the interval, thus the particle is far from making a full oscillation in each interval, anyway. In fact, the lower the amplitude A_n compared to the interval length (along the particle motion direction), the stronger the warp of the trajectory on this interval that may occur (see Figs. 2 and 3).

III. PARTICLE REFLECTION

A. Reflection conditions for positive particles

It is clear that the decrease of amplitudes (27) cannot continue indefinitely, because eventually arguments of the arcsines in (28) shall exceed unity [that happens sooner than the radicand in (27) becomes negative]. This merely signals that the particle cannot reach the next interplanar interval. The particle will continue its harmonic motion until it hits the previous interval, then proceed moving outward in the radial variable in the same but reverse way, and on the exit from the crystal it will emerge as a deflected beam.

Let us evaluate the order number $n_{\max}^{(+)}$ of the reflection interval. If, for some n, the inequality $\frac{d}{2}+\delta \leqslant A_{n-1}$ is met, then it also entails $\frac{d}{2}-\delta \leqslant A_n$, so the arguments of all the arcsines in (29) are less than unity. So, $n_{\max}^{(+)}$ is the largest integer yet allowing for $\frac{d}{2}-\delta \leqslant A_{n_{\max}^{(+)}}$. Through (27), that condition determines the reflection interval order number:

$$n_{\max}^{(+)} = \left\lfloor \frac{\tau^2\theta_0^2 + (b+\delta)^2 - \left(\frac{d}{2}-\delta\right)^2}{2\delta d}\right\rfloor, \tag{30}$$

where the lower-corner brackets $\lfloor\ldots\rfloor$ designate the integer part of a number ($\lfloor a\rfloor \leqslant a$). If $\tau\theta_0 \gg d$, the variation of $n_{\max}(b)$ is much smaller than its mean value, estimated as

$$n_{\max} \sim \frac{\tau^2\theta_0^2}{2\delta d} = \frac{R}{2d}\theta_0^2 \tag{31}$$

(this estimate is valid for negative particles as well; see Eq. (51) below). It is instructive to notice that

$$\frac{d}{2} - \delta \leqslant A_{n_{\max}^{(+)}} < \frac{d}{2} + \delta.$$

Toward the volume reflection problem, we are interested in finding the total reflection angle θ_{refl}, half of which, by symmetry reasons, amounts to the deflection angle of the trajectory in the reflection point $t = t_{\text{refl}}$ in which

$$\dot{r}(t_{\text{refl}}) = 0. \tag{32}$$

I.e.,

$$\frac{1}{2}\theta_{\text{refl}} \simeq \dot{x}(t_{\text{refl}}) = -\theta_0 + \delta\frac{t_{\text{refl}}}{\tau^2} \tag{33}$$

[more exactly, see Eq. (52) below].[8] To evaluate the right-hand side of (33), one only needs to know the value of t_{refl}. The latter is found from solving equation $\dot{r}(t_{\text{refl}}) = 0$:

$$\begin{aligned}\frac{t_{\text{refl}}}{\tau} &= \frac{t_{n_{\max}^{(+)}}}{\tau} + \frac{\pi}{2} \\ &= \frac{\pi}{2} + \sum_{n=1}^{n_{\max}^{(+)}} \left(\arcsin \frac{\frac{d}{2}+\delta}{A_{n-1}} + \arcsin \frac{\frac{d}{2}-\delta}{A_n} \right) \\ &\quad - \arcsin \frac{b+\delta}{A_0}.\end{aligned} \tag{34}$$

The largest contribution to the emerging sum comes from the terms $n \sim n_{\max}^{(+)}$ (where denominators A_n are smallest), so it may be more convenient here to revert the summation order. Introducing a useful parameter

$$\nu^{(+)} = \left\{ \frac{\tau^2\theta_0^2 + (b+\delta)^2 - \left(\frac{d}{2}-\delta\right)^2}{2\delta d} \right\}_{\text{f}}, \tag{35}$$

with braces $\{\ldots\}_{\text{f}}$ to indicate the fractional part ($0 \leqslant \nu^{(+)} < 1$), one recasts (34) as

$$\begin{aligned}\frac{t_{\text{refl}}}{\tau} &= \frac{\pi}{2} - \arcsin \frac{b+\delta}{\sqrt{\left(\frac{d}{2}-\delta\right)^2 + 2(\nu^{(+)} + n_{\max}^{(+)})\delta d}} \\ &\quad + \sum_{n=0}^{n_{\max}^{(+)}-1} \left(\arcsin \frac{\frac{d}{2}+\delta}{\sqrt{\left(\frac{d}{2}+\delta\right)^2 + 2(\nu^{(+)} + n)\delta d}} \right. \\ &\quad \left. + \arcsin \frac{\frac{d}{2}-\delta}{\sqrt{\left(\frac{d}{2}-\delta\right)^2 + 2(\nu^{(+)} + n)\delta d}} \right).\end{aligned} \tag{36a}$$

Equivalently, using the identity $\arcsin \frac{1}{\sqrt{1+\eta}} = \operatorname{arccot}\sqrt{\eta}$, one can write

$$\begin{aligned}\frac{t_{\text{refl}}}{\tau} &= \frac{\pi}{2} - \arcsin \frac{b+\delta}{\sqrt{\left(\frac{d}{2}-\delta\right)^2 + 2(\nu^{(+)} + n_{\max}^{(+)})\delta d}} \\ &\quad + \sum_{n=0}^{n_{\max}^{(+)}-1} \left(\operatorname{arccot} \frac{\sqrt{2(\nu^{(+)}+n)\delta d}}{\frac{d}{2}+\delta} \right. \\ &\quad \left. + \operatorname{arccot} \frac{\sqrt{2(\nu^{(+)}+n)\delta d}}{\frac{d}{2}-\delta} \right).\end{aligned} \tag{36b}$$

The physical meaning of parameter $\nu^{(+)}$ is clear from Fig. 2. It represents the kinetic transverse energy at the last atomic plane before the reflection, in units of the centrifugal potential difference between the neighboring atomic planes.

B. Negative particles

In contrast to the trigonometric arcsine, the hyperbolic arcsine function exists at any value of its argument. Therefore, expression (26) for negatively charged particle trajectories holds until the radicand in the motion amplitude A_n given by (27) becomes negative. The first interval at which that happens will be called the "inflection" one. Its order number is inferred to be

$$n_{\text{infl}} = \left\lfloor \frac{\tau^2\theta_0^2 - (b-\delta)^2}{2\delta d} \right\rfloor + 1. \tag{37}$$

In the inflection interval, the amplitude $A_{n_{\text{infl}}}$ calculated by the formula (27) would be imaginary. That implies that the $r(t)$ dependence now is to be described by a hyperbolic cosine rather than a sine. Matching the amplitude and the phase of the hyperbolic cosine with solution (26) for the preceding $n = n_{\text{infl}} - 1$ gives

$$\begin{aligned}r_{n_{\text{infl}}}(t) &= -\delta - n_{\text{infl}}d + |A_{n_{\text{infl}}}| \cosh \left(\frac{t}{\tau} + \varphi_0 + \sum_{m=1}^{n_{\text{infl}}-1} \Delta\varphi_m \right. \\ &\quad \left. - \operatorname{arsinh} \frac{\frac{d}{2}-\delta}{A_{n_{\text{infl}}-1}} - \operatorname{arcosh} \frac{\frac{d}{2}+\delta}{|A_{n_{\text{infl}}}|} \right),\end{aligned} \tag{38}$$

valid at

$$\frac{d}{2} - n_{\text{infl}}d \leqslant r_{n_{\text{infl}}} \leqslant \frac{d}{2} - n_{\text{infl}}d,$$

with

$$\begin{aligned}|A_{n_{\text{infl}}}| &= \sqrt{-\tau^2\theta_0^2 + (b-\delta)^2 + 2n_{\text{infl}}\delta d} \\ &\equiv \sqrt{2\delta d(1-\nu^{(-)})},\end{aligned} \tag{39}$$

and

$$\nu^{(-)} = \left\{ \frac{\tau^2\theta_0^2 - (b-\delta)^2}{2\delta d} \right\}_{\text{f}}. \tag{40}$$

Since $\frac{d}{2} + \delta \geqslant \sqrt{2\delta d}$, the argument of arcosh in (38) is always $\geqslant 1$.

Next, the question arises, at which condition can the trajectory (38) actually reach the next interval, i.e., $r_{n_{\text{infl}}}(t)$

[8] Strictly speaking, the trajectory will not be exactly symmetric with respect to t_{refl} because the distances from t_{refl} to the crystal boundaries are in general different. However, contributions to θ_{refl} from crystal regions away from t_{refl} are supposed to decrease sufficiently rapidly, and one expects existence of a "thick-crystal limit" of θ_{refl}, relevant in actual practice; see Sec. IV. In this paper, we content ourselves with only the "volume" contribution (33) to θ_{refl} and do not study any boundary effects. As we shall see later (Sec. IV and Appendix), however, the omission of boundary effects requires certain care.

can descend to value $n_{\rm infl}d-\frac{d}{2}$. Since, by Eq. (40), $r_{n_{\rm infl}}(t)\geqslant -\delta-n_{\rm infl}d+|A_{n_{\rm infl}}|$, that would require

$$\delta-\frac{d}{2}>|A_{n_{\rm infl}}|. \tag{41}$$

Substituting here (39), and solving with respect to the ratio $\frac{\delta}{d}$, one may present (41) in the form

$$\frac{\delta}{d}\equiv\frac{R_c}{2R}>f(\nu^{(-)}), \tag{42}$$

with

$$f(\nu^{(-)})=\frac{3}{2}-\nu^{(-)}+\sqrt{(2-\nu^{(-)})(1-\nu^{(-)})}. \tag{43}$$

Function $f(\nu^{(-)})$ decreases monotonously (almost linearly) from $f(0)=\frac{3}{2}+\sqrt{2}\approx 2.9$ to $f(1)=\frac{1}{2}$.

In the simplest case illustrated in Fig. 3, when condition (42) is violated (e.g., if $\frac{\delta}{d}<\frac{1}{2}\leqslant f$), (37) must be the last interval reached by the particle, its order number being

$$n_{\rm max}^{(-)}=n_{\rm infl}=\left\lfloor\frac{\tau^2\theta_0^2-(b-\delta)^2}{2\delta d}\right\rfloor+1\quad\left(\text{if }\frac{\delta}{d}\leqslant f(\nu^{(-)})\right). \tag{44}$$

Expressing $t_{\rm refl}$ from equation $\dot r(t_{\rm refl})=0$ then gives

$$\frac{t_{\rm refl}}{\tau}=\operatorname{arcosh}\frac{\frac{d}{2}+\delta}{|A_{n_{\rm infl}}|}-\operatorname{arsinh}\frac{b-\delta}{A_0}+\sum_{n=0}^{n_{\rm infl}-1}\operatorname{arsinh}\frac{\frac{d}{2}-\delta}{A_n}+\sum_{n=1}^{n_{\rm infl}-1}\operatorname{arsinh}\frac{\frac{d}{2}+\delta}{A_n}. \tag{45}$$

Reversal of the summation order here leads to the expression

$$\frac{t_{\rm refl}}{\tau}=\operatorname{arcosh}\frac{\frac{d}{2}+\delta}{\sqrt{2\delta d(1-\nu^{(-)})}}-\operatorname{arsinh}\frac{b-\delta}{A_0}+\sum_{n=0}^{n_{\rm infl}-1}\operatorname{arsinh}\frac{\frac{d}{2}-\delta}{\sqrt{2\delta d(\nu^{(-)}+n)}}+\sum_{n=0}^{n_{\rm infl}-2}\operatorname{arsinh}\frac{\frac{d}{2}+\delta}{\sqrt{2\delta d(\nu^{(-)}+n)}}. \tag{46}$$

Therethrough, using Eq. (33), results the deflection angle.

Otherwise, i.e., if (42) holds (e.g., if $\frac{\delta}{d}>3>f$), in all the subsequent intervals after (37) the trajectory must also be expressed through hyperbolic cosines:

$$r_n(t)=-\delta-nd+|A_n|\cosh\left(\frac{t}{\tau}+\varphi_0+\sum_{m=1}^{n_{\rm infl}-1}\Delta\varphi_m-\operatorname{arsinh}\frac{\frac{d}{2}-\delta}{A_{n_{\rm infl}-1}}-\operatorname{arcosh}\frac{\frac{d}{2}+\delta}{|A_{n_{\rm infl}}|}-\sum_{m=n_{\rm infl}+1}^{n}\operatorname{arcosh}\frac{\frac{d}{2}+\delta}{|A_m|}+\sum_{m=n_{\rm infl}}^{n-1}\operatorname{arcosh}\frac{-\frac{d}{2}+\delta}{|A_m|}\right), \tag{47}$$

with amplitudes A_n still given by Eq. (27). Expression (47) is valid at

$$-\frac{d}{2}-nd\leqslant r_n\leqslant\frac{d}{2}-nd,\quad n\geqslant n_{\rm infl}.$$

Sequence (47) may continue as long as the arguments of all arcosh exceed unity, i.e., as long as

$$\frac{d}{2}+\delta\geqslant|A_n|, \tag{48}$$

which is equivalent to $-\frac{d}{2}+\delta\geqslant|A_{n-1}|$. Inserting here (27), one ultimately infers the value of the reflection interval order number:

$$n_{\rm max}^{(-)}=\left\lfloor\frac{\tau^2\theta_0^2-(b-\delta)^2+\left(\frac{d}{2}+\delta\right)^2}{2\delta d}\right\rfloor\quad\left(\text{if }\frac{\delta}{d}>f(\nu^{(-)})\right). \tag{49}$$

The above expression is similar to Eq. (30) for positively charged particles. As one might expect, in the high-energy limit $\delta\gg d,b$, values $n_{\rm max}^{(+)}$ and $n_{\rm max}^{(-)}$ coincide and do not depend on the particle energy.

Expressing $t_{\rm refl}$ from $\dot r(t_{\rm refl})=0$ and Eq. (47) in this case gives

$$\frac{t_{\rm refl}}{\tau}=-\operatorname{arsinh}\frac{b-\delta}{A_0}+\sum_{n=0}^{n_{\rm infl}-1}\operatorname{arsinh}\frac{\frac{d}{2}-\delta}{A_n}+\sum_{n=1}^{n_{\rm infl}-1}\operatorname{arsinh}\frac{\frac{d}{2}+\delta}{A_n}+\sum_{m=n_{\rm infl}}^{n_{\rm max}^{(-)}}\operatorname{arcosh}\frac{\frac{d}{2}+\delta}{|A_m|}-\sum_{m=n_{\rm infl}}^{n_{\rm max}^{(-)}-1}\operatorname{arcosh}\frac{-\frac{d}{2}+\delta}{|A_m|},$$

or, reverting the summation order

$$\frac{t_{\rm refl}}{\tau}=-\operatorname{arsinh}\frac{b-\delta}{\sqrt{2\delta d(n_{\rm infl}-1+\nu^{(-)})}}+\sum_{n=0}^{n_{\rm infl}-1}\operatorname{arsinh}\frac{\frac{d}{2}-\delta}{\sqrt{2\delta d(\nu^{(-)}+n)}}+\sum_{n=0}^{n_{\rm infl}-2}\operatorname{arsinh}\frac{\frac{d}{2}+\delta}{\sqrt{2\delta d(\nu^{(-)}+n)}},+\sum_{n=1}^{n_{\rm max}^{(-)}-n_{\rm infl}+1}\operatorname{arcosh}\frac{\frac{d}{2}+\delta}{\sqrt{2\delta d(n-\nu^{(-)})}}-\sum_{n=1}^{n_{\rm max}^{(-)}-n_{\rm infl}}\operatorname{arcosh}\frac{-\frac{d}{2}+\delta}{\sqrt{2\delta d(n-\nu^{(-)})}}. \tag{50}$$

Actually, Eq. (50) can be used not only under condition (42), but also at any ratio $\frac{\delta}{d}$, provided that in capacity of $n_{\rm max}^{(-)}$ one uses the expression

$$n_{\rm max}^{(-)}=\left\lfloor\frac{\tau^2\theta_0^2-(b-\delta)^2+\left(\frac{d}{2}-\delta\right)^2\Theta\left(\frac{\delta}{d}-f(\nu^{(-)})\right)}{2\delta d}\right\rfloor+1 \tag{51}$$

(with $\Theta(v)$ the Heavyside unit-step function), unifying (44) and (49).[9] The universally valid formula (51) may be

[9]Evidently, expression (51) at $\frac{\delta}{d}>f$ reduces to (49), whereas at $\frac{\delta}{d}<f$ it turns to (44), with the last sum of (50) vanishing and the

convenient when $t_{\rm refl}$ is evaluated with the aid of a computer for widely varying values of particle energy or crystal bending radius.

As for the physical meaning of $\nu^{(-)}$ – at $\frac{\delta}{d} < f$, i.e., when the inflection interval is also that of reflection, Fig. 3 illustrates that the meaning of $\nu^{(-)}$ is similar to that of $\nu^{(+)}$. It is the (appropriately rescaled) kinetic transverse energy upon the particle entrance to the reflection interplanar interval, only the interval boundary now is not the atomic plane but the last potential maximum passed. If $\frac{\delta}{d} > f$, then $\nu^{(-)}$ does not characterize the reflection interval, and vice versa, the kinetic energy in the reflection interval is not closely related with $\nu^{(-)}$.

The obtained expressions (26)–(29) for the trajectory and (36) and (50) for its reflection point open prospects for evaluation of all the observables relevant to the particle passage. In the present paper, we will be interested only in the final angle of elastic reflection.

C. Thick-crystal limit (isolation of volume effects)

Formulas (36) and (50), in principle, contain dependencies on both volume and boundary effects. In most practical cases, the deflecting crystal may be regarded as thick, whence boundary effects are expected to become negligible. An increase of the crystal thickness, or more precisely, of the distance between the crystal boundary and the volume reflection point, may be thought of as an increase of the particle incidence angle θ_0 (see Fig. 1). Then, it suffices to consider the limit

$$\theta_{\rm refl} \approx \theta_{\rm v.r.} = 2 \lim_{\theta_0/\theta_c \to \infty} \left(-\theta_0 + \delta \frac{t_{\rm refl}(\theta_0)}{\tau^2} \right). \qquad (52)$$

With function (36), or (50), such a limit must always be finite. Indeed, at large $n_{\max}$ the sum over n grows as the corresponding integral, whose asymptotic behavior straightforwardly evaluates as

$$\frac{t_{\rm refl}}{\tau} \sim \int^{n_{\max}} dn \left(\frac{\frac{d}{2}+\delta}{\sqrt{2(\nu^{(+)}+n)\delta d}} + \frac{\frac{d}{2}-\delta}{\sqrt{2(\nu^{(+)}+n)\delta d}} \right)$$
$$\sim \sqrt{\frac{2n_{\max}d}{\delta}} \simeq \theta_0 \frac{\tau}{\delta}.$$

This leading asymptotic behavior cancels exactly the first term in (52), while calculation of the finite remainder requires a more accurate evaluation of the sum, which will be our task in the next section (in application to limit $R \gg R_c$).

In general, it must be noted that function $\theta_{\rm v.r.}(\tau,\delta,d,b)$, being a dimensionless function of four dimensional variables, may depend only on their three dimensionless ratios, say, d/τ, δ/d, and b/d. At that, the last ratio is always ~ 1. The first ratio amounts to

$$\frac{d}{\tau} = \sqrt{\frac{2d}{R_c}} = 2\theta_c, \qquad (53)$$

next-to-last sum reducing to a single term, equal to the first term of Eq. (46).

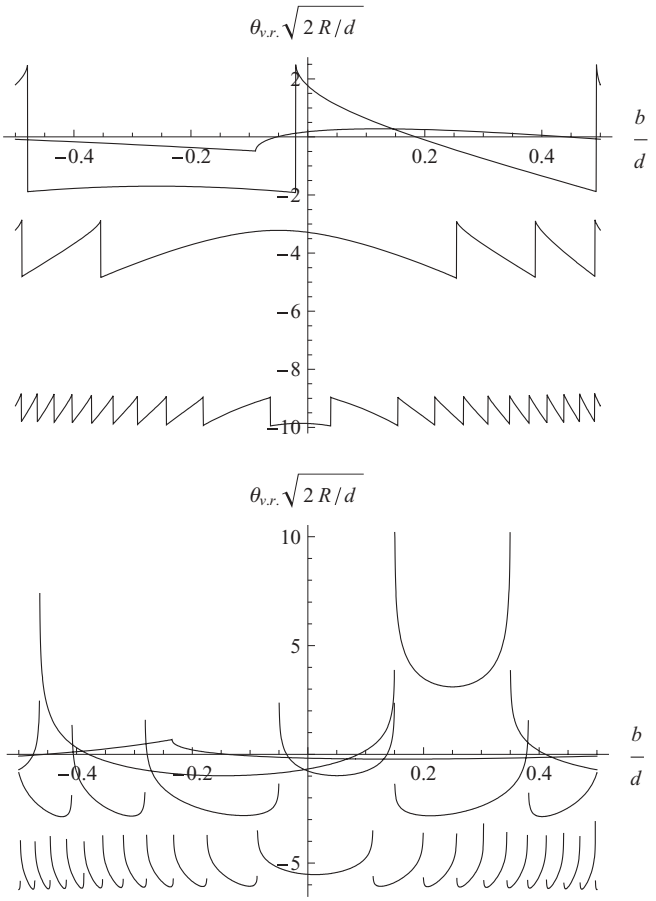

FIG. 4. The volume reflection angle $\theta_{\rm v.r.}$ as a function of impact parameter b, for $R/R_c = 1/3,2,10,40$. Top panel: for positively charged particles. Bottom panel: for negatively charged particles. Beyond the shown unit interval of b/d the whole picture repeats periodically.

where θ_c is the Lindhard critical angle [8]; so, it is always small, once we are in a high-energy regime. As for the ratio

$$\frac{2\delta}{d} = \frac{R_c}{R}, \qquad (54)$$

it may be either large or small depending on the particle energy and the crystal bending radius. The regime of particle passage through the crystal is determined solely by ratio (54).

To gain a general impression of the functional dependencies involved, and to test our generic formulas (36) and (50), let us view the dependence $\theta_{\rm v.r.}(b)$ for different values of R/R_c. Figure 4 shows this dependence for positive and for negative particles. They are in fair agreement with Figs. 6 and 8 of [11]. But we will pay more attention to interpretation of the features observed in the figures:

(1) The origin of the recurrent structure in variable b with a tapering period is, obviously, due to $\theta_{\rm v.r.}$ dependence on b through $\nu^{(\pm)}$ alone [see Eqs. (35) and (40)], insofar as $\nu^{(\pm)}$, involving an operation of fractional part, is a periodic function of $\frac{(b\pm\delta)^2}{2\delta d}$, which in the interval $-\frac{d}{2} < b < \frac{d}{2}$ makes $\sim 2\frac{d^2}{8\delta d} = \frac{R}{2R_c} \gg 1$ periods. Physically, it owes to the fact that variation of the particle initial potential energy, after the entrance to the crystal, at $R > R_c$ is greater than the energy

shift between the neighboring potential barriers. Also, since $\nu^{(\pm)}$ is an even function of $b \pm \delta$, the particle deflection angle is a symmetric function of b with respect to point $b = -\delta$ for positively charged particles, and with respect to $b = \delta$ for negative particles.

(2) Another feature of $\theta_{\text{v.r.}}(b)$ dependencies is that, for *negatively* charged particles, the reflection angle blows up (formally) to $+\infty$ at certain values of impact parameters. Physically, that corresponds to close matching of the particle transverse energy to the height of a (locally parabolic) effective potential barrier—the situation known as orbiting (see [12]).[10] The asymptotics of the divergences is logarithmic [12], as follows from the general integral expression of the deflection angle in a central potential $V(r)$:[11]

$$\theta \underset{E\gg m}{\approx} 2M\int_{r_{\min}}^{\infty}\frac{dr/(R+r)^2}{\sqrt{[E-V(r)]^2-M^2/(R+r)^2}}-\pi \tag{55a}$$

$$\underset{R\gg r,b}{\approx}\frac{1}{R}\int_{r_{\min}}^{\infty}\frac{dr}{\sqrt{\frac{\theta_0^2}{4}+\frac{V_{\text{eff}}(-b)-V_{\text{eff}}(r)}{2E}}}-\pi \tag{55b}$$

$$\underset{|\Delta E_\perp|\ll|F_{\max}|d}{\sim}\theta_c\frac{4\delta}{d}\int\limits_{|r-r_{\text{saddle}}|\lesssim d}\frac{dr}{\sqrt{\frac{d\Delta E_\perp}{|F_{\max}|}+(r-r_{\text{saddle}})^2}}+\cdots \tag{55c}$$

$$\simeq\theta_c\frac{4\delta}{d}\begin{cases}\ln\frac{1}{\nu^{(-)}}+\cdots & (\Delta E_\perp\propto\nu^{(-)}\to+0),\\ \frac{1}{2}\ln\frac{1}{1-\nu^{(-)}}+\cdots & (\Delta E_\perp\propto\nu^{(-)}-1\to-0).\end{cases} \tag{55d}$$

Here

$$M\simeq(R-b)[E-V(b)]\left(1-\theta_0^2/2\right)$$

is the particle angular momentum relative to the crystal bend axis,

$$V_{\text{eff}}(r)=V(r)-E\frac{r}{R} \tag{56}$$

is the effective potential including the centrifugal energy, r_{saddle} is the position of the maximum of the effective potential barrier whose height in the case of orbiting happens to be close to the particle energy, and $\Delta E_\perp$ is the departure of the transverse energy

$$E_\perp(\theta_0,b)=\frac{E}{2}\theta_0^2+V_{\text{eff}}(-b)=\frac{F_{\max}}{d}\left[A_0^2(\theta_0,b)+\delta^2\right] \tag{57}$$

from the top of the closest effective potential barrier. The factor $\frac{1}{2}$ in the $\Delta E_\perp<0$ alternative of Eq. (55d) arises because the integration in (55c) is then restricted to the one-sided neighborhood of r_{saddle}, where the radicand stays positive (see Fig. 5).

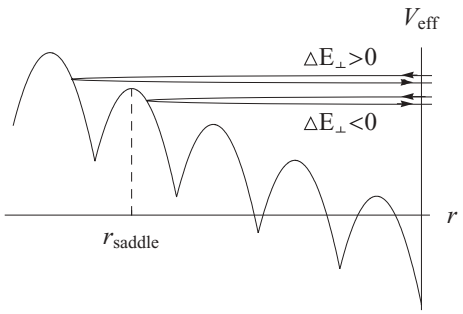

FIG. 5. The relation between the particle transverse energy and the effective potential energy V_{eff} (including the centrifugal potential) under the conditions of *negatively* charged particle orbiting in a bent crystal. The leading logarithmic contribution to integral (55b) comes from the vicinity of point r_{saddle}, the coordinate of the effective potential maximum to which the particle transverse energy happens to be close. In the case $\Delta E_\perp > 0$, the particle sweeps the two-sided neighborhood of r_{saddle}, whereas at $\Delta E_\perp < 0$, it sweeps the one-sided neighborhood only.

(3) It must be noticed that for negative particles, function $\theta_{\text{v.r.}}(b)$ has stationary points (smooth minima), which must correspond to caustics, i.e., to rainbow scattering [12].

(4) For positive particles, in contrast, the potential in its maximum is not differentiable, excluding both orbiting and rainbow scattering phenomena for this case. With some smearing of the potential around the atomic planes, these effects will, of course, reappear. But on the other hand, they may be reduced by intense incoherent multiple scattering in this region.

A proper question is whether it is possible to derive, at least, the particle final deflection angle (related to $\frac{t_{\text{refl}}}{\tau}$) from the more conventional integral representation approach [2,9]. In that approach, momentum and transverse energy conservation laws are incorporated automatically, so there is no need to connect trajectories on the interval borders. Indeed, specializing in (56) and (55b)

$$V(r)=F_{\max}d\left(\frac{r}{d}+n\right)^2,\quad n=-\left\lfloor\frac{r}{d}+\frac{1}{2}\right\rfloor \tag{58}$$

(at $r>0$ n is nonnegative; $n(r=-b)=0$), and using the basic integral

$$\int_{-d/2-nd}^{d/2-nd}\frac{dr}{\sqrt{\tau^2\theta_0^2+b^2+2\delta(b+r)-(r+nd)^2}}$$
$$=\arcsin\frac{\frac{d}{2}-\delta}{\sqrt{\tau^2\theta_0^2+(b+\delta)^2-2n\delta d}}$$
$$+\arcsin\frac{\frac{d}{2}+\delta}{\sqrt{\tau^2\theta_0^2+(b+\delta)^2-2n\delta d}} \tag{59}$$

for positively charged particles, and a similar one for negative particles, we reproduce the inverse trigonometric and hyperbolic functions encountered in (34), (46), and (50). But the integral representation approach would not directly give us explicit trajectories $r(t)$ [rather, $t(r)$, to be solved for r],

[10]The verbal description of this effect for negative particle case is contained in [2] (end of Sec. 3), and a graphical illustration thereof appears in [9] (Fig. 5, trajectory 2). But the relation with the general concept of orbiting (spiral scattering), as formulated in [12], was only noticed in [13]. We refrain from discussion of possible experimental significance of orbiting here.

[11]Equation (55a) agrees with our definition of the θ angle, usual in volume reflection studies, and differs in sign from the conventional in mechanics definition of deflection angle in a centrally symmetric field.

and the geometric interpretation (Figs. 2 and 3) would not be immediate.

On the other hand, from the integral representation for the final angle, we might derive the result in the form of a sum of analytic functions also for a more complicated parametrization of the interplanar potential, e.g., adding a term proportional to r^4. Then instead of arcsines, one would encounter elliptic functions. But it is the simplicity of the functions under the sum that permits us, in the important limit $R \gg R_c$, when the number of terms in the sum grows large, to replace the sums by integrals and to do the latter ones in closed form. In this sense, analytic investigation only *begins* at the present stage.

IV. VOLUME REFLECTION REGIME (MODERATELY HIGH ENERGIES, $R \gg R_c$)

As we had mentioned in the Introduction, and as Fig. 4 does confirm, under the condition $R \gg R_c$, i.e., $2\delta \ll d$, the particle deflection angle depends weakly on the impact parameter. So, it is interesting, in the first place, to determine the numerical value of the limiting ratio $\lim_{R/R_c\to\infty} \frac{\theta_{\text{v.r.}}}{\theta_c}$. Second, it is desirable to determine the final beam shape and quantify its angular width as a function of R/R_c. That will be our aim in this section. The treatment is somewhat different for the cases of positively and negatively charged particles, because of the difference between the functional form of initial Eqs. (36) and (50).

A. Positive particles

For positively charged particles, in the considered limiting case $\delta \ll d$, say, quantity $(\frac{d}{2} \pm \delta)^2 + 2(\nu^{(+)} + n)\delta d$ entering the denominators in (36a) varies relatively little as n changes from n to $n+1$. Thus, there must be a possibility to replace the summation in (36) by integration. The proper mathematical tool for that is the Euler-Maclaurin formula (see, e.g., [14]) which reads

$$\sum_{n=0}^{N} f(n) = \frac{1}{2} f(0) + \int_0^N dn f(n) + \frac{1}{2} f(N) + O\left(\frac{df}{dn}\right). \tag{60}$$

Employing this formula for approximation of each of the sums in (36b) [the latter being somewhat more convenient than Eq. (36a)], one gets[12]

$$\begin{aligned}\sum_{n=0}^{n_{\max}^{(+)}-1} &\operatorname{arccot}\frac{\sqrt{2\delta d(\nu^{(+)}+n)}}{\frac{d}{2}\pm\delta} \\ &= \frac{1}{2}\operatorname{arccot}\frac{\sqrt{2\delta d\nu^{(+)}}}{\frac{d}{2}\pm\delta} + \int_{\nu^{(+)}}^{n_{\max}^{(+)}+\nu^{(+)}-1} dn \operatorname{arccot}\frac{\sqrt{2\delta dn}}{\frac{d}{2}\pm\delta} \\ &\quad + \frac{1}{2}\operatorname{arccot}\frac{\sqrt{2\delta d(n_{\max}^{(+)}+\nu^{(+)}-1)}}{\frac{d}{2}\pm\delta} + O\left(\sqrt{\frac{\delta}{d}}\right), \end{aligned} \tag{61}$$

[12]In this subsection, the sign alternative in $\frac{d}{2} \pm \delta$ corresponds to dealing with the first or with the second of the sums in (36b).

where we had estimated, for all n,

$$\left|\frac{d}{dn}\operatorname{arccot}\frac{\sqrt{2\delta d(\nu^{(+)}+n)}}{\frac{d}{2}\pm\delta}\right| \lesssim \sqrt{\frac{\delta}{d}}.$$

The two end-point contributions in (61) are small as $O(\delta/d)$ relative to the integral, but still they need to be kept if we wish to describe not only the mean deflection, but also the scattered beam shape.

Taking the indefinite integral in Eq. (61) by parts,

$$\int dn \operatorname{arccot}\sqrt{an} = \frac{1}{a}[(1+an)\operatorname{arccot}\sqrt{an} + \sqrt{an}],$$

one brings (61) to the form

$$\begin{aligned}\sum_{n=0}^{n_{\max}^{(+)}-1} &\operatorname{arccot}\frac{\sqrt{2\delta d(\nu^{(+)}+n)}}{\frac{d}{2}\pm\delta} \\ &\underset{\delta\ll d}{\approx} \frac{\left(\frac{d}{2}\pm\delta\right)^2}{2\delta d}\left[\left(1+\frac{2\delta d}{\left(\frac{d}{2}\pm\delta\right)^2}(n_{\max}^{(+)}+\nu^{(+)}-1)\right)\right. \\ &\quad\times\operatorname{arccot}\frac{\sqrt{2\delta d(n_{\max}^{(+)}+\nu^{(+)}-1)}}{\frac{d}{2}\pm\delta} \\ &\quad+\frac{\sqrt{2\delta d(n_{\max}^{(+)}+\nu^{(+)}-1)}}{\frac{d}{2}\pm\delta} - \left(1+\frac{2\delta d\nu^{(+)}}{\left(\frac{d}{2}\pm\delta\right)^2}\right) \\ &\quad\left.\times\operatorname{arccot}\frac{\sqrt{2\delta d\nu^{(+)}}}{\frac{d}{2}\pm\delta} - \frac{\sqrt{2\delta d\nu^{(+)}}}{\frac{d}{2}\pm\delta}\right] + \frac{1}{2}\operatorname{arccot}\frac{\sqrt{2\delta d\nu^{(+)}}}{\frac{d}{2}\pm\delta} \\ &\quad+\frac{1}{2}\operatorname{arccot}\frac{\sqrt{2\delta d(n_{\max}^{(+)}+\nu^{(+)}-1)}}{\frac{d}{2}\pm\delta} + O\left(\sqrt{\frac{\delta}{d}}\right). \end{aligned} \tag{62}$$

In the limit $n_{\max}^{(+)} \to \infty$, with the use of asymptotic expansion $\operatorname{arccot}\sqrt{\eta} = \frac{\pi}{2} - \sqrt{\eta} + O(\eta^{3/2})$, expression (62) reduces to

$$\begin{aligned}\sum_{n=0}^{n_{\max}^{(+)}-1} &\operatorname{arccot}\frac{\sqrt{2\delta d(\nu^{(+)}+n)}}{\frac{d}{2}\pm\delta} \\ &\underset{n_{\max}^{(+)}\gg 1}{\to} \frac{d\pm 2\delta}{\sqrt{2\delta d}}\sqrt{n_{\max}^{(+)}} - \frac{\left(\frac{d}{2}\pm\delta\right)^2}{2\delta d} \\ &\quad\times\left[\left(1+\frac{2\delta d}{\left(\frac{d}{2}\pm\delta\right)^2}\right)\left(\frac{\pi}{2}-\frac{\sqrt{2\delta d\nu^{(+)}}}{\frac{d}{2}\pm\delta}\right)+\frac{\sqrt{2\delta d\nu^{(+)}}}{\frac{d}{2}\pm\delta}\right] \\ &\quad+\frac{1}{2}\frac{\pi}{2} + O\left(\frac{1}{\sqrt{n_{\max}^{(+)}}}, \sqrt{\frac{\delta}{d}}\right). \end{aligned} \tag{63}$$

Here, one notices that the terms $-\frac{\sqrt{2\delta d\nu^{(+)}}}{\frac{d}{2}\pm\delta}$, $+\frac{\sqrt{2\delta d\nu^{(+)}}}{\frac{d}{2}\pm\delta}$ in the brackets in (63) cancel. Further on, inserting (63) to (36b) and this to (52), we witness the anticipated cancellation of the large

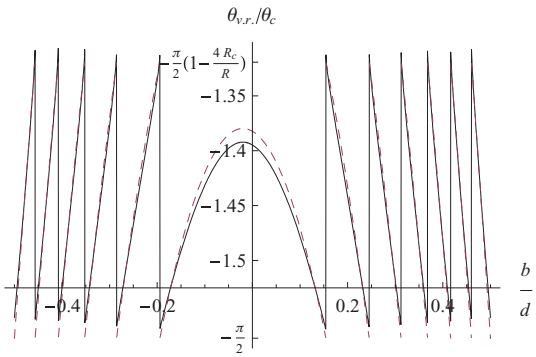

FIG. 6. (Color online) Solid curve shows the positively charged particle deflection angle $\theta_{\text{v.r.}}$ vs impact parameter b, for $R/R_c = 25$. Dashed curve is approximation (64). The central segments of the curves are strongly θ_0 dependent.

terms $-\theta_0 + \frac{\sqrt{2\delta d}}{\tau} n_{\max}^{(+)} \cong 0$, and ultimately arrive at a result

$$\begin{aligned}\theta_{\text{v.r.}}(b) \approx & -2\theta_0 + 2\frac{\delta}{\tau}\left[\frac{\pi}{2} + \frac{2d}{\sqrt{2\delta d}}\sqrt{n_{\max}^{(+)}}\right. \\ & -\frac{\pi}{2}\left(\frac{\left(\frac{d}{2}+\delta\right)^2}{2\delta d} + \nu^{(+)}\right) + \frac{\pi}{4} \\ & \left.-\frac{\pi}{2}\left(\frac{\left(\frac{d}{2}-\delta\right)^2}{2\delta d} + \nu^{(+)}\right) + \frac{\pi}{4}\right] \\ \equiv & -\frac{\pi}{2}\theta_c\left[1 - \frac{4R_c}{R}[1-\nu^{(+)}(b)] + O\left(\frac{R_c^{3/2}}{R^{3/2}}\right)\right],\end{aligned} \tag{64}$$

remembering that $\nu^{(+)}(b)$ is given by Eq. (35).

Comparison of approximation (64) with the exact result (36) is shown in Fig. 6. (Actually, the given approximation appears to be numerically accurate starting from $R/R_c \sim 5$). From the figure [or Eq. (64)], one concludes that in the first approximation, all the particles are deflected to the same angle $\approx -\frac{\pi}{2}\theta_c$. There is also some dispersal of the scattering angles, depending on the particle impact parameter, of the full width equal to

$$\Delta\theta_{\text{v.r.}} = \theta_c \frac{2\pi R_c}{R} \equiv \frac{2\pi\delta}{\tau} \quad \text{(positively charged particles)}, \tag{65}$$

The observable quantity, however, is not the indicatrix $\theta_{\text{v.r.}}(b)$ but the scattering differential cross section (final particle flux averaged over the impact parameters b) as a function of the scattering angle $\theta_{\text{v.r.}}$. Therefore, it is desirable to reconstruct the latter dependence issuing from the first. Fortunately, that does not pose any principal problem, granted the linearity of the dependence $\theta_{\text{v.r.}}(\nu^{(+)})$.

1. Differential cross section

Turning to the evaluation of the differential cross section, one encounters a certain complication: the b-dependent quantity $\nu^{(+)}$ in (64) also contains a dependence on θ_0. The fact of residual θ_0 dependence was previously noticed in [11]. To some degree, it conflicts with our initial assumption about the boundary condition vanishing influence in the limit of large θ_0/θ_c. We cannot revoke it at the present stage, since in Eq. (52) we had already incorporated the facilitating assumption of the trajectory symmetry with respect to point t_{refl}. Obviously, the sensitivity to the boundary conditions in general destroys such a symmetry. Moreover, θ_{refl} might as well contain a dependence on the particle *exit angle* relative to the atomic planes, which we did not even take trouble to specify. Fortunately, the impediment is not fatal and curable within the present framework. In principle, the sensitivity of the differential cross section to θ_0 is attenuated with the increase of R/R_c, but more importantly, we will prove that upon averaging over a *tiny* interval of θ_0 this dependence is eliminated completely.

To begin with, the differential cross section involves only a *derivative* of function $\theta_{\text{v.r.}}(b)$:

$$\begin{aligned}\frac{d\lambda}{d\theta_{\text{v.r.}}} &= \sum_m \frac{1}{|d\theta_{\text{v.r.}}/db|_{b=b_m(\theta_{\text{v.r.}})}} \\ &\equiv \frac{R}{2\pi\theta_c R_c}\sum_m \frac{1}{|d\nu^{(+)}/db|_{b=b_m(\nu^{(+)}(\theta_{\text{v.r.}}))}},\end{aligned} \tag{66}$$

where $b_m(\theta)$ is the set of all the roots of equation $\theta_{\text{v.r.}}(b) = \theta$ belonging to the interval $-\frac{d}{2} < b < \frac{d}{2}$. Now, at $R/R_c \gg 1$ the number of roots b_m to equation $\theta_{\text{v.r.}} = \theta$ is large, and so, in general, they are densely distributed over the finite definition interval $-\frac{d}{2} < b < \frac{d}{2}$. It appears that the root distribution density is just proportional to the derivative in the denominator of (66) (the formal demonstration is relegated to the Appendix). Therefore, the sum appearing in (66) is approximately equal to just the b variation interval length, i.e., d. Still, the relation expected thereby,

$$\frac{d\lambda}{d\theta_{\text{v.r.}}} \simeq \frac{Rd}{2\pi\theta_c R_c}, \tag{67}$$

does not yet hold *uniformly* in b, and hence in $\theta_{\text{v.r.}}$. For instance, in the neighborhood of point $b = -\delta$ we have in the denominator of (66) $\partial\nu^{(+)}/\partial b \to 0$ (see Fig. 6), so there the differential cross section blows up above the plateau (67) (see Appendix). But the latter peak position on the $\theta_{\text{v.r.}}$ axis depends sharply on the value of θ_0 and hence is essentially "random" and needing to be averaged over.

In this connection, notice that the dependence of $\nu^{(+)}$ on θ_0 is quadratic, so a situation is possible in which the incident particle beam divergence is smaller than the angular spread acquired in the crystal:

$$\Delta\theta_0 \ll \Delta\theta_{\text{v.r.}}, \tag{68}$$

but at the same time, the indeterminance of $\frac{\tau^2\theta_0^2}{2\delta d} \approx n_{\max}^{(+)}$ is greater than unity:

$$\Delta\left(\frac{\tau^2\theta_0^2}{2\delta d}\right) = \frac{\tau^2\theta_0}{\delta d}\Delta\theta_0 \gg 1. \tag{69}$$

Together, Eqs. (68) and (69) may be viewed as a double inequality:

$$\frac{2\delta}{\tau}\frac{\theta_c}{\theta_0} \ll \Delta\theta_0 \ll \frac{2\pi\delta}{\tau} \quad (\theta_0\text{-averaging}). \tag{70}$$

Here, the sufficient gap exists provided

$$\theta_0 \ggg \frac{\theta_c}{\pi}. \tag{71}$$

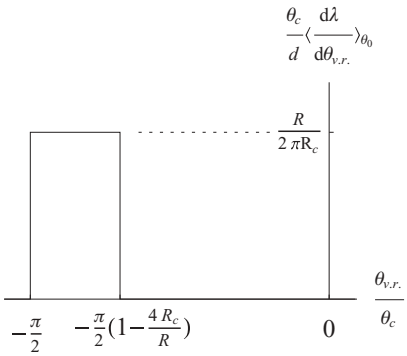

FIG. 7. Asymptotic (at $R \gg R_c$) behavior of the θ_0-averaged differential cross section for positively charged particle scattering [Eq. (72)]. The area under the rectangular curve is unity, representing the total probability. In higher orders in R_c/R the distribution edges must smear out (see discussion in the text).

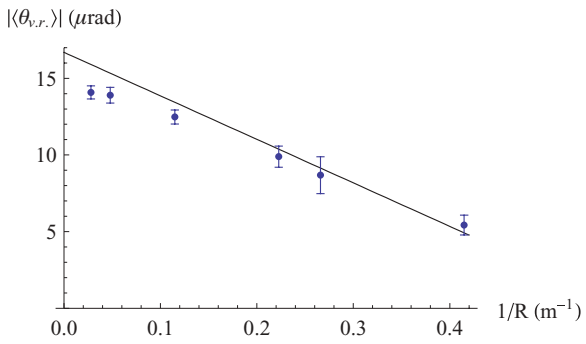

FIG. 8. Mean volume reflection angle dependence on the crystal curvature, at $E = 400$ GeV, for silicon crystal in orientation (111). Points: experimental data from [15]. Line: prediction of Eq. (73), with parameters evaluated as explained in the text.

This is basically the same condition that we had assumed at writing Eq. (52); thus for derivation of a θ_0-averaged differential cross section, we can safely rely on Eq. (64).

Ultimately, we can make a specific statement that under conditions (70), upon θ_0-averaging, the differential cross section equals to constant value (67) over an interval where roots b_m exist. This interval is rather obvious from Eq. (64)—its ends correspond to ends of $\nu^{(+)}$ variation interval: $\nu^{(+)} = 0$ corresponds to $\theta_{\text{v.r.}} = -\frac{\pi}{2}(1 - \frac{4R_c}{R})$, and $\nu^{(+)} = 1$ corresponds to $\theta_{\text{v.r.}} = -\frac{\pi}{2}$ [see also Appendix, Eq. (A12)]. So, the θ_0-averaged differential cross section (the final beam profile) is described by a simple rectangular function

$$\left\langle \frac{d\lambda}{d\theta_{\text{v.r.}}} \right\rangle_{\theta_0} \approx \frac{Rd}{2\pi\theta_c R_c}\Theta\left(\theta_{\text{v.r.}} + \frac{\pi}{2}\theta_c\right) \times \Theta\left(-\theta_{\text{v.r.}} - \frac{\pi}{2}\theta_c\left(1 - \frac{4R_c}{R}\right)\right), \quad (72)$$

see Fig. 7.

2. *Comparison with experiment*

When comparing our model result for the final beam profile with experiments, an important issue is the significance of incoherent multiple scattering with the targets of ~1 mm used to date. Deferring the numerical estimates till Sec. VI, note that the deflection angle mean value must be least affected by multiple scattering; so, it may offer a clean experimental test. From (64), we obviously infer

$$\langle\theta_{\text{v.r.}}\rangle = -\frac{\pi}{2}\theta_c\left(1 - \frac{2R_c}{R}\right) \equiv -\frac{\pi}{2}\sqrt{\frac{d}{2R_c}}\left(1 - \frac{2R_c}{R}\right). \quad (73)$$

The property of (73) is the linearity of the dependence on the crystal curvature R^{-1}; the linear kind of the dependence was indeed noticed in CERN experiments with $E = 400$ GeV [15].

To make a quantitative comparison with the experiment, one needs to specify the potential strength in our model. In reality, the Si(110) interplanar potential is characterized by two parameters: $F_{\max} \approx 6$ GeV/cm (usually used for evaluation of R_c for channeling conditions) and the well depth $V_0 = 22.7$ eV (usually used for evaluation of the critical angle θ_c for volume reflection). The relation $V_0 = \frac{1}{4}F_{\max}d$ implied by a quadratic potential model only holds with accuracy ≈ 25%:

$$22.7\,\text{eV} = V_0 \neq \tfrac{1}{4}F_{\max}d = 28.8\,\text{eV},$$
$$d = 1.92\ \text{Å for Si(110)}.$$

If we evaluate R_c in (73) as $R_c = E/F_{\max} = 0.67$ m, it will produce too large $|\langle\theta_{\text{v.r.}}\rangle|$. But evaluating both R_c and θ_c as $R_c = \frac{Ed}{4V_0} \approx 0.85$ m, $\theta_c = \sqrt{2V_0/E} \approx 11\mu$rad, and substituting into Eq. (73), we get a satisfactory agreement with the experiment (see Fig. 8).

As for the obtained rectangular profile shape, it is more sensitive to multiple scattering, and has not yet been cleanly accessed in experiments (the optimal experimental conditions will be specified in Sec. VI). But we can compare our profile with the available numerical simulation results using a realistic, thermally smeared potential, and neglecting multiple scattering, too: Ref. [9], Fig. 6. In that case, the positive particle profile shows indeed a signature of flattening ("shoulder") but near its edges the distribution behaves differently, exhibiting a subtle divergence (rainbow) at the outer edge, and decreasing continuously on the inward side. So, for positively charged particles our simplified model of parabolic interplanar potential describes the final beam *profile* only qualitatively, though it is able to predict the distribution width and mean value.

Next, turning to the negative particle reflection problem, we shall see that in this case our analytic approach is able to appropriately describe the final beam profile edge detail even.

B. Negative particles

In the case of negative particles, the starting point is Eq. (46) [relevant under (strong) condition (42)], and again, it has to be examined with the object of trading the sum for an integral. First, we must mind that at $n \sim 1$ the hyperbolic arcsine arguments vary significantly; but at the same time, they are large, while the hyperbolic arcsine of a large argument is close to the logarithm of a large argument, i.e., $\text{arsinh}\upsilon \simeq_{\upsilon\gg 1} \ln 2\upsilon$, and thus varies relatively little. On the other hand, in the domain of large n the arguments of the arcsines vary little. Therefore, over the *entire* summation interval, both sums involved may be approximated by integrals. Yet, the first terms in the sums are singular functions of $\nu^{(-)}$, and therefore are

better taken into account separately. Thereafter, application of the Euler-Maclaurin formula to the first of the sums in Eq. (46) gives

$$\begin{aligned}\sum_{n=0}^{n_{\rm infl}-1} &\operatorname{arsinh}\frac{\frac{d}{2}-\delta}{\sqrt{2\delta d(\nu^{(-)}+n)}}\\ &\approx \ln\frac{d-2\delta}{\sqrt{2\delta d\nu^{(-)}}}+\frac{1}{2}\ln\frac{d-2\delta}{\sqrt{2\delta d(\nu^{(-)}+1)}}\\ &\quad+\int_{\nu^{(-)}+1}^{\nu^{(-)}+n_{\rm infl}-1} dn\,\operatorname{arsinh}\frac{\frac{d}{2}-\delta}{\sqrt{2\delta d}\sqrt{n}}\\ &\quad+\frac{1}{2}\operatorname{arsinh}\frac{\frac{d}{2}-\delta}{\sqrt{2\delta d(\nu^{(-)}+n_{\rm infl}-1)}}.\end{aligned}\tag{74}$$

The next-to-leading order (derivative-related) correction term [14] to (74) amounts to

$$\frac{1}{12}\frac{d}{dn}\operatorname{arsinh}\frac{\frac{d}{2}-\delta}{\sqrt{2\delta d(\nu^{(-)}+n)}}\Bigg|_{n=1}^{n=n_{\rm infl}-1}\approx-\frac{1}{24(1+\nu^{(-)})}.\tag{75}$$

We will omit it because of the smallness of the numerical coefficient $\frac{1}{24}$, although, in principle, asymptotically it is also relevant [the same is true for all the higher derivatives, whose contributions enter with yet smaller coefficients (involving inverse factorial and Bernoulli numbers)].

Next, calculating the indefinite integral in Eq. (74) by parts,

$$\int dn\,\operatorname{arsinh}\frac{a}{\sqrt{n}}=n\,\operatorname{arsinh}\frac{a}{\sqrt{n}}+a\sqrt{a^2+n},\tag{76}$$

we bring (74) to the form

$$\begin{aligned}\sum_{n=0}^{n_{\rm infl}-1} &\operatorname{arsinh}\frac{\frac{d}{2}-\delta}{\sqrt{2\delta d}\sqrt{\nu^{(-)}+n}}\\ &\approx(\nu^{(-)}+n_{\rm infl}-1)\operatorname{arsinh}\frac{\frac{d}{2}-\delta}{\sqrt{2\delta d(\nu^{(-)}+n_{\rm infl}-1)}}\\ &\quad+\frac{\frac{d}{2}-\delta}{\sqrt{2\delta d}}\sqrt{\frac{\left(\frac{d}{2}-\delta\right)^2}{2\delta d}+\nu^{(-)}+n_{\rm infl}-1}\\ &\quad-(1+\nu^{(-)})\operatorname{arsinh}\frac{\frac{d}{2}-\delta}{\sqrt{2\delta d(1+\nu^{(-)})}}\\ &\quad-\frac{\frac{d}{2}-\delta}{\sqrt{2\delta d}}\sqrt{\frac{\left(\frac{d}{2}-\delta\right)^2}{2\delta d}+1+\nu^{(-)}}\\ &\quad+\ln\frac{d-2\delta}{\sqrt{2\delta d\nu^{(-)}}}+\frac{1}{2}\ln\frac{d-2\delta}{\sqrt{2\delta d(1+\nu^{(-)})}}\\ &\quad+\frac{1}{2}\operatorname{arsinh}\frac{\frac{d}{2}-\delta}{\sqrt{2\delta d(\nu^{(-)}+n_{\rm infl}-1)}}.\end{aligned}\tag{77}$$

Now, in the thick-crystal limit $n_{\rm infl}\to\infty$, Eq. (77) simplifies to

$$\begin{aligned}\sum_{n=0}^{n_{\rm infl}-1} &\operatorname{arsinh}\frac{\frac{d}{2}-\delta}{\sqrt{2\delta d}\sqrt{\nu^{(-)}+n}}\\ &\underset{n_{\rm infl}\gg1}{\to}\sqrt{n_{\rm infl}}\frac{d-2\delta}{\sqrt{2\delta d}}-(1+\nu^{(-)})\ln\frac{d-2\delta}{\sqrt{2\delta d(1+\nu^{(-)})}}\\ &\quad-\frac{\left(\frac{d}{2}-\delta\right)^2}{2\delta d}\sqrt{1+\frac{2\delta d}{\left(\frac{d}{2}-\delta\right)^2}(1+\nu^{(-)})}\\ &\quad+\ln\frac{d-2\delta}{\sqrt{2\delta d\nu^{(-)}}}+\frac{1}{2}\ln\frac{d-2\delta}{\sqrt{2\delta d(1+\nu^{(-)})}}\\ &\cong\sqrt{n_{\rm infl}}\frac{d-2\delta}{\sqrt{2\delta d}}-\left(\frac{1}{2}+\nu^{(-)}\right)\ln\frac{d-2\delta}{\sqrt{2\delta d(1+\nu^{(-)})}}\\ &\quad-\frac{\left(\frac{d}{2}-\delta\right)^2}{2\delta d}-\frac{1}{2}(1+\nu^{(-)})+\ln\frac{d-2\delta}{\sqrt{2\delta d\nu^{(-)}}}.\end{aligned}\tag{78}$$

Similarly, the second term in (46) reduces to

$$\begin{aligned}\sum_{n=0}^{n_{\rm infl}-2} &\operatorname{arsinh}\frac{\frac{d}{2}+\delta}{\sqrt{2\delta d(\nu^{(-)}+n)}}\\ &\to\sqrt{n_{\rm infl}}\frac{d+2\delta}{\sqrt{2\delta d}}-\left(\frac{1}{2}+\nu^{(-)}\right)\ln\frac{d+2\delta}{\sqrt{2\delta d(1+\nu^{(-)})}}\\ &\quad-\frac{\left(\frac{d}{2}+\delta\right)^2}{2\delta d}-\frac{1}{2}(1+\nu^{(-)})+\ln\frac{d+2\delta}{\sqrt{2\delta d\nu^{(-)}}}.\end{aligned}\tag{79}$$

Inserting (78) and (79) into Eqs. (46) and thereupon to (52), after a simple rearrangement, one is left with the final result:

$$\begin{aligned}\theta_{\rm v.r.}\approx-\theta_c\Bigg[1-\frac{2R_c}{R}&\left(\frac{1}{2}\ln\frac{1}{e(1-\nu^{(-)})}+\ln\frac{1}{\nu^{(-)}}\right.\\ &\left.-\left(\nu^{(-)}+\frac{1}{2}\right)\ln\frac{e}{(1+\nu^{(-)})}+(1-\nu^{(-)})\ln\frac{R}{R_c}\right)\Bigg],\end{aligned}\tag{80}$$

where the definition for $\nu^{(-)}(b)$ is Eq. (40). Note that logarithmic asymptotics of this expression at $\nu^{(-)}\to0$ and at $\nu^{(-)}\to1$ agrees with the general law (55d).

The exact (52) versus approximate (80) expressions for the indicatrix $\theta_{\rm v.r.}\big(\nu^{(-)}(b)\big)$ are compared in Fig. 9.

1. Differential cross section

To deduce the observable differential cross section from the available indicatrix, we have again to issue from Eq. (66).

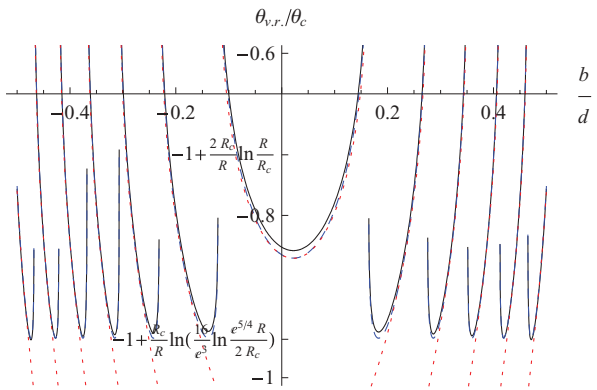

FIG. 9. (Color online) Comparison of the exact formulas (52) and (46) for the negatively charged particle indicatrix (black solid curve) with the approximation (80) (blue dashed curve) and approximation (90) (red dotted curve), for $R/R_c=25$. The central segments of the curves are strongly θ_0 dependent.

To some extent, the same procedure as for positively charged particles applies here, leading to the representation

$$\frac{d\lambda}{d\theta_{\mathrm{v.r.}}} = \sum_{j=1}^{2} \left| \frac{d\nu^{(-)}}{d\theta_{\mathrm{v.r.}}} \right| \sum_{m} \frac{1}{|\partial \nu_j^{(-)}/\partial b|} \Bigg|_{b=b_m(\nu_j^{(-)}(\theta_{\mathrm{v.r.}}))}, \tag{81}$$

where $b_m(\nu^{(-)})$ is the solution of Eq. (40), and $\sum_{j=1}^{2}$ accounts for the existence of two roots to equation $\theta_{\mathrm{v.r.}} = \theta_{\mathrm{v.r.}}(\nu^{(-)})$ with the function (80). Again, upon averaging over θ_0 under condition (70) (cf. Appendix), one obtains

$$\frac{1}{d}\left\langle \frac{d\lambda}{d\theta_{\mathrm{v.r.}}} \right\rangle_{\theta_0} = \sum_{j=1}^{2} \left| \frac{d\nu_j^{(-)}}{d\theta_{\mathrm{v.r.}}} \right|, \tag{82}$$

i.e., averaging over b (and a tiny interval of θ_0) reduces to averaging over $\nu^{(-)}$ (transverse energy). Note that when $\nu^{(-)}$ becomes a uniformly distributed random quantity in a unit variation interval, for each given b, and thus for a certain $\theta_{\mathrm{v.r.}}$, one can always unambiguously tell whether $\nu^{(-)} = \nu_1^{(-)}$ or $\nu^{(-)} = \nu_2^{(-)}$, so the probability normalization is conserved under conditions of summation over the branches.

A technical distinction of the case with negative particles is that Eq. (80) cannot be resolved with respect to $\nu^{(-)}$ in an explicit and exact form. Of course, it can be easily solved numerically; the differential cross section so evaluated is shown in Fig. 10, by a solid curve. On the other hand, it is also useful to pursue an analytic but approximate approach, based on different approximations in different regions of $\nu^{(-)}$, which will require some additional effort.

2. *Asymptotic evaluation of the final beam profile*

In Eq. (80) at typical $\nu^{(-)}$ the leading term is the last one, where $\nu^{(-)}$ is multiplied by a large logarithm. Besides that, in the domain of $\nu^{(-)}$ close to 1 the first logarithm in (80) turns large, too, and a minimum of function $\theta_{\mathrm{v.r.}}(\nu^{(-)})$ emerges,

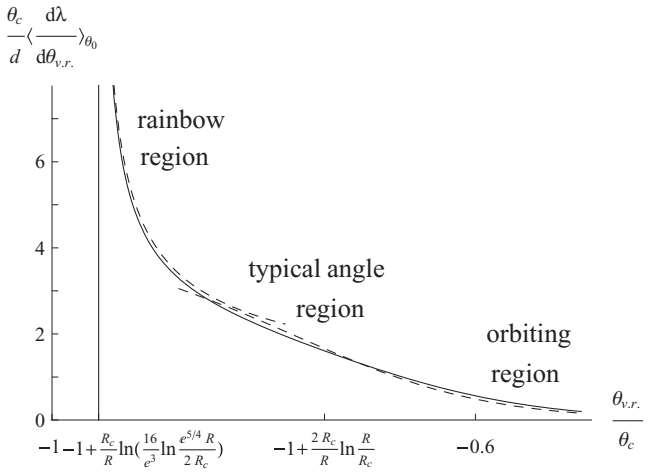

FIG. 10. The θ_0-averaged differential cross section of negatively charged particle scattering, at $R/R_c = 25$ (solid curve). The axes scales are chosen so that the area under the curve is unity, as the total probability. The left-hand dashed curve is evaluated by the explicit approximate formula (87); the right-hand dashed curve–by the explicit approximate formula (94). It is observed that these two approximations actually overlap.

corresponding to the onset of rainbow scattering. As for the second logarithm in (80), which raises at $\nu^{(-)} \to 0$, it does not lead to formation of a minimum in the $\theta_{\mathrm{v.r.}}(\nu^{(-)})$ dependence; on the contrary, it makes the dependence steeper, and in the area of its significance the differential cross section is small (exponentially). So, for the description of the differential cross section, it basically suffices to consider only two regions: the region where the last term of (80) dominates, and the region where the last term and $\frac{1}{2}\ln\frac{1}{e(1-\nu^{(-)})}$ in (80) are competing. On the $\theta_{\mathrm{v.r.}}$ axis, the mentioned regions are adjacent, and conjointly they should give almost the full picture of the variation of the differential cross section. For completeness, one may consider also a third, asymptotic region of the "tail" of the differential cross section (orbiting region), where the first and second logarithms of (80) dominate.

a. Rainbow region. The value of $\nu^{(-)}$ corresponding to the rainbow angle is to be determined from the condition

$$\left.\frac{\partial\theta_{\mathrm{v.r.}}}{\partial\nu^{(-)}}\right|_{\nu^{(-)}=\nu_0^{(-)}} = 0, \tag{83}$$

which in application to expression (80) gives

$$\frac{\nu_0^{(-)}}{1-\nu_0^{(-)2}} - \frac{1}{\nu_0^{(-)}} + \ln\left(1+\nu_0^{(-)}\right) = \ln\frac{R}{R_c} \gg 1. \tag{84}$$

The approximate solution of Eq. (84) is

$$\nu_0^{(-)} \approx 1 - \frac{1}{2\ln\frac{e^{5/4}R}{2R_c}} + O\left(\frac{1}{\ln^3\frac{e^{5/4}R}{2R_c}}\right). \tag{85}$$

In the vicinity of the found point $\nu_0^{(-)}$ we may expand function $\theta_{\mathrm{v.r.}}(\nu^{(-)})$ up to a quadratic term:

$$\left(\frac{\theta_{\mathrm{v.r.}}}{\theta_c}+1\right)\frac{R}{2R_c} \approx \frac{1}{2}\ln\left(\frac{16}{e^3}\ln\frac{e^{5/4}R}{2R_c}\right) + (\nu^{(-)}-\nu_0^{(-)})^2\ln^2\frac{e^{5/4}R}{2R_c} + O\left((\nu^{(-)}-\nu_0^{(-)})^3\ln^3\frac{e^{5/4}R}{2R_c}\right). \tag{86}$$

Now, expressing the pair of roots $\nu_j^{(-)}(\theta_{\mathrm{v.r.}})$ from the quadratic equation (86), one derives by formula (81) the behavior of the θ_0-averaged differential cross section in the vicinity of the rainbow angle:

$$\frac{\theta_c}{d}\left\langle\frac{d\lambda}{d\theta_{\mathrm{v.r.}}}\right\rangle_{\theta_0} \approx \frac{\sqrt{R/2R_c}}{\ln\frac{e^{5/4}R}{2R_c}\sqrt{\frac{\theta_{\mathrm{v.r.}}}{\theta_c}+1-\frac{R_c}{R}\ln\left(\frac{16}{e^3}\ln\frac{e^{5/4}R}{2R_c}\right)}}. \tag{87}$$

The domain of applicability of this approximation is determined from Eq. (86) by demanding the third-order term to be small compared with the second-order one:

$$\left(\frac{\theta_{\mathrm{v.r.}}}{\theta_c}+1\right)\frac{R}{R_c} - \ln\left(\frac{16}{e^3}\ln\frac{e^{5/4}R}{2R_c}\right) \ll 1 \quad \text{(rainbow region)}. \tag{88}$$

Function (87) is shown by the left-hand dashed curve in Fig. 10.

b. Typical angle region. On the other hand, if $\nu^{(-)}$ is not too close to 1, i.e., under condition

$$\left(\frac{\theta_{\text{v.r.}}}{\theta_c}+1\right)\frac{R}{R_c}-\ln\left(\frac{16}{e^3}\ln\frac{e^{5/4}R}{2R_c}\right)\gtrsim 1 \quad \text{(typical angles)} \tag{89}$$

opposite to (88), all the terms in (80) except the second logarithm (singular at $\nu^{(-)}\to 0$) may reasonably be approximated by their Taylor expansions up to linear terms, say, about the unit interval midpoint $\nu^{(-)}_{\text{mid}}=\frac{1}{2}$:[13]

$$\theta_{\text{v.r.}}\approx-\theta_c\left[1-\frac{2R_c}{R}\left(\ln\frac{\sqrt{3}R}{\nu^{(-)}R_c}-\frac{11}{6}-\nu^{(-)}\ln\frac{2R}{3e^{2/3}R_c}\right)\right]. \tag{90}$$

Then, for determination of the inverse function $\nu^{(-)}(\theta_{\text{v.r.}})$ one obtains the following simplified equation:

$$\left(\frac{\theta_{\text{v.r.}}}{\theta_c}+1\right)\frac{R}{2R_c}+\frac{11}{6}\approx\ln\frac{\sqrt{3}R}{\nu^{(-)}R_c}-\nu^{(-)}\ln\frac{2R}{3e^{2/3}R_c}. \tag{91}$$

Here, the right-hand side is a monotonic function of $\nu^{(-)}$, so, in contrast to the exact equation (80), the simplified equation (91) has only one root (the second, lost root gives a negligible contribution to the differential cross section). The solution to Eq. (91) is expressed through the Lambert (also known as product log) function $W(s)$ defined as a solution to equation $\ln s=\ln W+W$, and incorporated in many computational software packages:

$$\nu^{(-)}\approx\frac{1}{\ln\frac{2R}{3e^{2/3}R_c}}W\left(\frac{\sqrt{3}R\ln\frac{2R}{3e^{2/3}R_c}}{R_c}e^{-\frac{11}{6}-\frac{R}{2R_c}\left(\frac{\theta_{\text{v.r.}}}{\theta_c}+1\right)}\right). \tag{92}$$

(Mind that $\theta_{\text{v.r.}}/\theta_c$ is negative and close to -1.) From the definition of W, its asymptotic behavior in different regions derives as

$$W(s)=\begin{cases}s-O(s^2), & (s\ll 1),\\ \ln\frac{s}{\ln\frac{s}{\cdots}}, & (s\gg 1),\end{cases} \tag{93}$$

and its derivative

$$W'(s)=\frac{1}{s[1+1/W(s)]}.$$

Therefore, over the typical angle region, the θ_0-averaged differential cross section is cast as

$$\frac{\theta_c}{d}\left\langle\frac{d\lambda}{d\theta_{\text{v.r.}}}\right\rangle_{\theta_0}=\theta_c\left|\frac{d\nu^{(-)}}{d\theta_{\text{v.r.}}}\right|\approx\frac{R}{2R_c\ln\frac{2R}{3e^{2/3}R_c}}\frac{1}{(1+1/W)}, \tag{94}$$

the argument of W being the same as in Eq. (92).

The full width of the differential cross section, as can be inferred from Eq. (94), and is obvious already from Eq. (80), amounts to

$$\Delta\theta_{\text{v.r.}}\sim\theta_c\frac{2R_c}{R}\ln\frac{R}{R_c} \quad \text{(negatively charged particles)}, \tag{95}$$

which at $R/R_c>e^{\pi}\approx 23$ is larger than width (65) for positively charged particles.

The behavior of function (94) in region (89) is shown in Fig. 10 by the right-hand dashed curve. It describes the actual distribution quite accurately. In the orbiting region asymptotics, however, Eq. (94) errs by a factor of $e^{5/6}/\sqrt{3}\approx 1.3$ [see Eq. (97) below], so the applicability of (94) is restricted by the bound

$$\frac{R}{2R_c}\left(\frac{\theta_{\text{v.r.}}}{\theta_c}+1\right)\lesssim\ln\frac{R}{R_c} \quad \text{(typical angles)},$$

in addition to (89).

One may anticipate formation of a shoulder in the distribution (94) at sufficiently large R/R_c, since then the argument of W can be large and $1+1/W\to 1$, making the differential cross section $\theta_{\text{v.r.}}$ independent. However, $W(s)$ reaches 5 ($\gg 1$) only at $s\sim 700$, so a shoulder in $\langle d\lambda/d\theta_{\text{v.r.}}\rangle_{\theta_0}$ may develop only at $R/R_c\gtrsim 100$.

c. Orbiting region. Finally, asymptotically large $\theta_{\text{v.r.}}$ are generated in the regions $\nu^{(-)}\to 0$ and $\nu^{(-)}\to 1$, where there are logarithmically rising terms in the relation (80). Examine first the region $\nu^{(-)}\to 0$. In this limit, one may let $\nu^{(-)}=0$ everywhere in (80) except in $\ln\frac{1}{\nu^{(-)}}$, and the reduced equation

$$\theta_{\text{v.r.}}\simeq-\theta_c\left(1-\frac{2R_c}{R}\ln\frac{R}{eR_c\nu^{(-)}}\right)$$

is easily solved:

$$\nu^{(-)}\simeq\frac{R}{eR_c}e^{-\frac{R}{2R_c}\left(\frac{\theta_{\text{v.r.}}}{\theta_c}+1\right)}. \tag{96}$$

Differentiating that expression with respect to $\theta_{\text{v.r.}}$, the asymptotics of the differential cross section results as

$$\frac{\theta_c}{d}\left\langle\frac{d\lambda}{d\theta_{\text{v.r.}}}\right\rangle_{\theta_0}\simeq\frac{R^2}{2eR_c^2}e^{-\frac{R}{2R_c}\left(\frac{\theta_{\text{v.r.}}}{\theta_c}+1\right)} \quad \text{(orbiting region)}, \tag{97}$$

holding if

$$\frac{R}{2R_c}\left(\frac{\theta_{\text{v.r.}}}{\theta_c}+1\right)\gg\ln\frac{R}{R_c} \quad \text{(orbiting region)}.$$

As for the contribution from region $\nu^{(-)}\to 1$, which can be treated in a completely analogous manner, it equals

$$\frac{8R}{e^4R_c}e^{-\frac{R}{R_c}\left(\frac{\theta_{\text{v.r.}}}{\theta_c}+1\right)},$$

and is definitely negligible compared to (97); so, Eq. (97) is the complete asymptotic result.

3. *Comparison with experiment*

The only measurement of negatively charged particle volume reflection is [4]. It gave, for Si (110) orientation, $R/R_c\approx 70$, the volume reflection angle mean value $|\langle\theta_{\text{v.r.}}\rangle|=0.66\theta_c$. This is significantly smaller than our expectation (and other simulations, as quoted in [16]) $|\langle\theta_{\text{v.r.}}\rangle|\approx\theta_c$ (yet minus $\sim$8% correction for finite R_c/R, which is insignificant anyway). Of course, if we treat $|F_{\max}|$ as an adjustable parameter of the model, we might achieve agreement with the experiment, but a physical recipe for this is not clear.

As for numerical calculation results for the final beam profile, there is a lack of them for negatively charged particles

[13] More elegant expressions, at the same time accommodating for a correct asymptotics in the orbiting region, result when the Taylor expansion is carried out about the point $\nu^{(-)}=0$; but unfortunately, that approximation would be definitely less accurate at typical $\theta_{\text{v.r.}}$.

at $R \gg R_c$ and free of multiple scattering (and with the boundary conditions congruent with typical experimental ones).[14] We hope to see such results in near future.

V. HIGH-ENERGY PASSAGE LIMIT (PERTURBATIVE DEFLECTION)

In conclusion, we will briefly comment on the behavior of the function $\theta_{\text{v.r.}}(b)$ in the opposite, high-energy limit

$$\frac{d}{2\delta} = \frac{R}{R_c} \ll 1. \tag{98}$$

There, the deflection becomes perturbative (and better viewed in Cartesian coordinates, without the reference to a centrifugal force notion), and for positive and negative particles it must be equal in magnitude but opposite in sign. That is confirmed by Figs. 4 and 11.

The specific expression for the dependence $\theta_{\text{v.r.}}(b)$ in this limit was obtained in [17] [Eqs. (16) and (19)], in the Cartesian coordinate framework:

$$\theta_{\text{v.r.}}(\theta_0,b) \to \theta_{\text{Born}}(\theta_0,b) = \frac{1}{E}\int_{-\infty}^{\infty} dz F(b,z) \tag{99a}$$

$$= \pm 4\frac{\sqrt{2Rd}}{R_c}\zeta\left(-\frac{1}{2},\left\{\frac{1}{2}+\frac{R}{2d}\theta_0^2+\frac{b}{d}\right\}_{\text{f}}\right) \tag{99b}$$

(again, the braces with subscript 'f' indicate taking the fractional part). It involves the Hurwitz (generalized Riemann) ζ function at a negative value of its first argument, which may be defined, e.g., as a contour integral [14]

$$\zeta(\alpha,v) = \frac{\Gamma(1-\alpha)}{2\pi i}\int_{-\infty}^{(0+)} \frac{s^{\alpha-1}e^{vs}}{1-e^s} ds \tag{100}$$

along a Hankel path.[15] Function (99b) is shown in Fig. 11 by the dotted line. Note the identity $\zeta(-\frac{1}{2},0) = \zeta(-\frac{1}{2},1)$ [$\equiv \zeta(-\frac{1}{2})$], whereby function (99b) is everywhere continuous, but its derivative breaks at point $\frac{b}{d} = \frac{1}{2} - \{\frac{R\theta_0^2}{2d}\}_{\text{f}}$.

The second argument of the ζ function in (99b) allows for a physical interpretation [17]:

$$b_{\text{refl}} = b + \frac{R}{2}\theta_0^2 \tag{101}$$

is the particle impact parameter at a depth where the particle straight trajectory becomes tangential to the bent atomic planes (actually, t_{refl}). Should one pass to b_{refl} instead of b, the dependence on θ_0 disappears completely:

$$\theta_{\text{v.r.}}(\theta_0,b) = \theta_{\text{v.r.}}(b_{\text{refl}}). \tag{102}$$

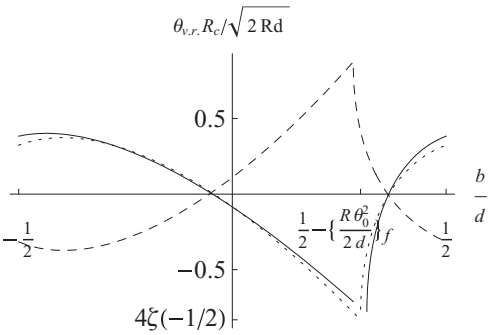

FIG. 11. Comparison of impact parameter dependencies of the reflection angle for positively charged (solid curve) and negatively charged (dashed curve) particles, at $R/R_c = 1/20$. Dotted curve: approximation (99b), for positive particles. The functions displayed may be continuously periodically extended beyond the interval $(-\frac{1}{2},\frac{1}{2})$. The position of the fracture at $\frac{b}{d} = \frac{1}{2} - \{\frac{R\theta_0^2}{2d}\}_{\text{f}}$ corresponds to tangency of the particle near-straight trajectory to one of the bent atomic planes.

This contrasts with the case $R \gg R_c$ investigated in the previous section, where the θ_0 dependence yet remained in a specific, casually located rainbow peak.

Here we will not contemplate demonstrating from expressions (36) and (50) that the limit of $\theta_{\text{v.r.}}$ is indeed (99b), only note that to this end, one must implement significant cancellations between the pair of terms under the sum sign. One also notices that the second argument of the ζ function in (99b) is just the limit of $\nu^{(+)}$:

$$\lim_{\delta/d\to\infty} \nu^{(+)} = \left\{\frac{1}{2}+\frac{R}{2d}\theta_0^2+\frac{b}{d}\right\}_{\text{f}}. \tag{103}$$

For negative particles, the route to (99b) is a bit more intricate. In Fig. 11, we numerically compare approximation (99b) with the exact result; the agreement is quite convincing.

The comparison with the perturbative scattering pattern may also give insight into the origin of the volume reflection phenomenon. The average of function (99) over the impact parameter b turns out to be strictly zero (see [17]); hence, in the high-energy limit, signatures of the volume reflection completely disappear. This is traced to the fact that $\int_{-d/2}^{d/2} dbF(b,z) \equiv 0$ at any given z (regardless of the crystal bend). In contrast, at $R \gtrsim R_c$ the trajectory may *not* be viewed as merely straight,[16] and the particle distribution is nonuniform over the crystal volume. In fact, "shadowed regions" not filled by the particles may appear at the inner side of bent potential ridges, in which the force acts in the positive direction. The

[14] Paper [9] does not exhibit negative particle results for $R > R_c$. In the pioneering work [2] the boundary conditions are different from ours and from typical experimental arrangements: the authors conduct their simulations for particles entering the crystal face parallel to the bent atomic planes (a "half" volume reflection). That should produce a different final beam shape (with no rainbow singularity and more particles in the "orbiting" tail), but nonetheless, Fig. 4(b) of [2] is visually rather similar to our Fig. 10.

[15] Conventionally, the Hankel path is defined to begin in the complex s plane at $-\infty$ ($\arg s = -\pi$), encircle the origin in the positive direction, and return to $-\infty$ ($\arg s = +\pi$).

[16] In the literature, sometimes, one encounters an interpretation of the volume reflection phenomenon simply in terms of a straight trajectory tangential to the bent crystalline planes in some point. Such an interpretation, although sufficient for an approximately symmetric installation of crystals with a large bending angle ($\sim 2\theta_0 \gg \theta_c$), may be misleading for understanding of the underlying particle dynamics.

deficit of a positively directed force on the beam then leads to the negative sign of the particle beam mean deflection angle.

VI. EXPERIMENTAL OBJECTIVES AND PARAMETER OPTIMIZATION

The alleged application of volume reflection is for high-energy particle beam extraction from accelerator beamlines, when that is not manageable within the lab space by means of magnets (whose fields are always much weaker than intra-crystalline electric fields). There, the beam parameters (energy and angular divergence) are definite, while the crystal parameters have to be optimized in order to attain a suitable deflection quality.

A. Control of beam divergence accompanying the deflection

The mean deflection angle

$$|\theta_{\text{v.r.}}| \sim \theta_c, \quad \theta_c = \sqrt{\frac{2V_0}{E}} \approx 21\mu\text{rad}\sqrt{\frac{100\ \text{GeV}}{E}} \tag{104}$$

for a silicon crystal of orientation (109) depends only on the particle energy. The next parameter to care about is the angular spread acquired by the beam at the exit from the crystal. Neglecting the incoherent multiple scattering (to be estimated below), the spread $\Delta\theta_{\text{v.r.}}$, given by Eqs. (65) and (95), for a given beam energy and crystal material depends only on the crystal bending radius. To derive a criterion for the beam complete deflection, one may demand that the bulk of the dispersed beam (its both "edges") be deflected to the same side. That implies

$$R > 4R_c \quad \text{(for positively charged particles)}, \tag{105}$$

and

$$R > 2R_c \ln\frac{R}{R_c} \quad \text{(for negatively charged particles)}. \tag{106}$$

Relation (105) involving the factor 4 was first found by Maisheev [9] based on numerical simulation studies for protons. Our paper, thereby, offers a formal justification for that empirical relation, although within a framework of a simplified model. The emerging ratio

$$\mathsf{q} = \frac{\max|\theta_{\text{v.r.}}|}{\Delta\theta_{\text{v.r.}}} = \begin{cases} \frac{R}{4R_c} & \text{(for pos. charged particles)}, \\ \frac{R}{2R_c \ln\frac{R}{R_c}} & \text{(for neg. charged particles)}, \end{cases} \tag{107}$$

quantifies the steering quality. But for the deflection to be neat, one should have a substantial q:

$$\mathsf{q} \gtrsim 3 \quad \text{(neat deflection)}, \tag{108}$$

entailing for the crystal curvature radius

$$R \gtrsim 10\text{–}15R_c. \tag{109}$$

In demonstrational experiments [3], the latter requirement was marginally satisfied.

B. Sufficient crystal thickness

The crystal thickness L is to be kept as low as possible in order to minimize the multiple scattering. However, a lower bound for L results from the requirement that the volume reflection has space to develop, i.e., the "thick-crystal limit" holds, in the sense of Sec. III C. To this end, the crystal bending half angle $\frac{L}{2R}$ needs be larger than the critical angle θ_c, which is L independent. Thus,

$$L \gg 2R\theta_c = \frac{R}{R_c}d\sqrt{\frac{E}{2V_0}} \approx \frac{R}{4R_c}3.6\ \mu\text{m}\sqrt{\frac{E}{\text{GeV}}} \tag{110}$$

(thick crystal, volume reflection saturation).

If we regard here $\frac{R}{4R_c} = \mathsf{q}$ as fixed, in general L grows with the energy. At $E \sim 10^2$–10^3 GeV (RHIC, Tevatron) the minimal thickness amounts only to (0.036–0.1 mm)q. Note that crystals as thin as 30 μm are manufacturable (as described in [18]). For $E \sim 10$ TeV (LHC) and $\mathsf{q} \sim 3$, the minimal L reaches the value of 1 mm.

C. Reduction of multiple scattering

To quantify the impact of incoherent, multiple scattering, we have to evaluate the characteristic ratio[17]

$$\frac{\theta_x^{\text{mult}}}{\theta_c} \approx \frac{13.6\ \text{MeV}}{\sqrt{2}E}\sqrt{\frac{L}{93.6\ \text{mm}}}\sqrt{\frac{E}{2V_0}} \approx 0.47\sqrt{\frac{100\ \text{GeV}}{E}\frac{L}{\text{mm}}} \quad \text{[Si(110)]}. \tag{111}$$

If the latter square root does not exceed unity (in experiments [3] it is ≈ 1), the multiple scattering does not spoil coherent beam deflection. We conclude that for $E \gtrsim 100$ GeV crystal lengths up to 2 mm are multiple-scattering safe, i.e., $\theta_x^{\text{mult}}/\theta_c < 1$.

Besides aggregate deflection, it would be interesting to experimentally investigate the intrinsic volume-reflected beam *shape*, and in particular to check the shape dependence on the particle charge sign (cf. Figs. 7 and 10). The main problem here is that at $\mathsf{q} \gg 1$ the final beam half divergence $\frac{1}{2}\Delta\theta_{\text{v.r.}}$ is $2\mathsf{q}$ times smaller than the mean deflection angle, and so is sooner overtaken by the multiple scattering, making the profile Gaussian and independent of the particle charge sign. To avoid that, one needs the condition

$$\frac{\theta_x^{\text{mult}}}{\frac{1}{2}\Delta\theta_{\text{v.r.}}} \sim 2\mathsf{q}\frac{\theta_x^{\text{mult}}}{\theta_c} \ll 1, \tag{112}$$

with $\theta_x^{\text{mult}}/\Delta\theta_{\text{v.r.}}$ to be inferred from Eq. (111). Hence, for the present purpose we should not strive for large q, granted that the final beam profile is not very sensitive to q at $\mathsf{q} > 1$. So, $\mathsf{q} \simeq 1.2$ seems to be large enough. Equally well, in order to raise the angular resolution we should use moderate energies. Say, $E = 50$ GeV is ultrarelativistic enough. To reduce multiple

[17] For the (rms, plane) multiple-scattering angle upon the particle over-barrier passage we crudely apply a formula for the scattering angle in an *amorphous* target made of the same material (silicon): $\theta_x^{\text{mult}} = \frac{13.6\ \text{MeV}}{\sqrt{2}E}\sqrt{\frac{L}{93.6\ \text{mm}}}$ (as quoted in [19]).

scattering, we can take a thin crystal with $L = 30\,\mu$m, which marginally satisfies (110). This gives $\theta_c \approx 3 \times 10^{-5}$ rad, $\Delta\theta_{\text{v.r.}} \approx 2.5 \times 10^{-5}$ rad, and $\frac{\theta_x^{\text{mult}}}{\frac{1}{2}\Delta\theta_{\text{v.r.}}} \approx 0.3$ (small enough). But one has to control the initial particle impact angles with an accuracy a few times better than $\Delta\theta_{\text{v.r.}}$. This may be difficult to achieve via the initial beam collimation alone, so one may need to apply event selection techniques (cf. [4]).

VII. SUMMARY

Based on the model of a purely parabolic continuous potential in a bent crystal, we have gained a lot of information about the volume reflection phenomenon, for positively and negatively charged particles. First, we have obtained an explicit expression (26) for particle trajectories. From the solution for the trajectory, in particular, we have derived the particle final deflection angle as a function of the particle impact parameter and energy, in the form of sums (36) and (50). The asymptotic behavior of those sums at $R \gg R_c$ was explored, and asymptotic values for the volume reflection angle were found. They equal: $-\frac{\pi}{2}\theta_c$ for positive particles, and $-\theta_c$ for negative particles. This agrees within $\sim$20% with the existing results of numerical simulation using more realistic continuous potentials [2,9] and with experiment for positive particles [3] (though there is an indication of worse agreement for negative particles [4]); 20% is about the same accuracy as for approximating the continuous potential by a parabola. Yet we have evaluated the next-to-leading-order correction in parameter R_c/R, which depends on the impact parameter, and after averaging over impact parameters, we determined the asymptotic shape of the final beam. This in particular yields the mean volume reflection angle dependence on R_c/R, which appears to be linear, in general agreement with experiment [15] (see Fig. 8).

In the course of our investigation of the final beam shape, we discovered various singularities in its profile, which actually depend on the particle charge sign. First of all, we had to deal with the problem that the final beam profile, in principle, may contain a visible admixture of boundary-dependent effects ("randomly" located peaks). However, we have proved the statement that boundary effects get completely erased in the differential cross section averaged over a tiny interval of incident angles θ_0 [condition (70)], or, analogously, due to a bit of multiple scattering before the volume reflection region. Therewith, the averaging over impact parameters becomes equivalent to averaging over parameters $\nu^{(\pm)}$ (i.e., transverse energy), and we were able to analytically deduce the final beam profile for positive and for negative particles. For negatively charged particles, it is asymmetric, exhibiting a spike on its outer edge, corresponding to the rainbow scattering, and an exponential tail on the inner side, corresponding to orbiting (Fig. 10). For positive particles, the final beam tends to a rectangular shape (Fig. 7). But in actual practice, with the account of continuous potential smearing in the vicinity of the atomic planes, a weak rainbow spike and orbiting tail are expected for positive particles, as well, though being deteriorated by incoherent multiple scattering.

Toward practical applications and further experimental investigations, we have made a few numerical estimates. They indicate that for usage of a bent crystal as a coherent beam deflector, one needs a relation between the main parameters:

$$\frac{L}{1\text{ mm}} < \frac{E}{100\text{ GeV}} < \frac{R}{\text{m}}, \left(\frac{20\,\mu\text{rad}}{\sigma_0}\right)^2$$

(σ_0 is the rms angular deviation in the initial beam). The better those inequalities are met, the higher is the deflection quality. If in future one becomes interested in investigating the final beam intrinsic *shape*, generated by the continuous potential alone, those inequalities must be satisfied strongly, but minding the existence of technical lower limits for L and σ_0. This suggests an optimal of energy about 50 GeV (see end of Sec. VI C); experiments are to be carried out simultaneously with particles of both charge signs ($e^{\pm}$, $\pi^{\pm}$).

There are many respects in which the model solution described herein can be improved. First, it is straightforward to add to the simple parabolic potential a second parabolic segment, either to round off the potential in vicinities of atomic planes, or to describe the potential of a Si crystal in (111) planar orientation, which is of practical importance, too. As a next step, at least a perturbative account of incoherent scattering processes is desirable. But at the same time, even in the present form, the theory (trajectories derived in Sec. II) seems suitable, e.g., for studies of electromagnetic radiation emitted by a volume-reflected particle.

APPENDIX: FORMAL PROCEDURE OF θ_0-AVERAGING

In Sec. IV A we had obtained, for positively charged particles, the scattering differential cross section in the form

$$\frac{d\lambda}{d\theta_{\text{v.r.}}} = \frac{R}{2\pi\theta_c R_c}\sum_m \frac{1}{|d\nu^{(+)}/db|_{b=b_m(\nu^{(+)}(\theta_{\text{v.r.}}),\theta_0)}}. \tag{A1}$$

Our objective now is to straightforwardly compute the sum involved here for the specific function $\nu^{(+)}(b,\theta_0)$ given by Eq. (35), first for an arbitrary θ_0, and then average it over θ_0, in order to justify our assertion that the combined averaging over b and θ_0 [within the tiny interval (70)] is equivalent to averaging over $\nu^{(+)}$.

To begin with, let us find the roots b_m explicitly. Equation (35) is equivalent to

$$\frac{\tau^2\theta_0^2 + (b+\delta)^2 - \left(\frac{d}{2}-\delta\right)^2}{2\delta d} = \nu^{(+)} + m, \tag{A2}$$

with m an integer, solution of which is straightforward:

$$b_m(\nu^{(+)},\theta_0) = -\delta \pm \sqrt{2\delta d(\nu^{(+)}+m) + \left(\frac{d}{2}-\delta\right)^2 - \tau^2\theta_0^2}. \tag{A3}$$

Here the sequence of m begins with a smallest integer m_0 at which the radicand in (A3) is yet positive, viz.,

$$m_0 = \left\lfloor \frac{\tau^2\theta_0^2 - \left(\frac{d}{2}-\delta\right)^2}{2\delta d} - \nu^{(+)} \right\rfloor + 1. \tag{A4}$$

The upper limit of m in Eq. (A3) equals to the largest integer at which yet $b < \frac{d}{2}$ [for a branch with the "+" sign in front of

the root in Eq. (A3)], and $b > -\frac{d}{2}$ (for a branch with the "–" sign). That yields, correspondingly, values

$$m_{\max 1} = \left\lfloor \frac{\tau^2\theta_0^2}{2\delta d} - \nu^{(+)} \right\rfloor, \tag{A5}$$

$$m_{\max 2} = m_{\max 1} + 1. \tag{A6}$$

The number of terms in the sums from limit (A4) to limit (A5) or (A6) is large:

$$m_{\max 1,2} - m_0 = \frac{d}{8\delta} + O(1) \equiv \frac{R}{4R_c} + O(1) \gg 1.$$

Next, values of derivative $\frac{d\nu^{(+)}}{db}$ in points b_m are easily evaluated, noticing that the fractional part operator in $\nu^{(+)}$ is inconsequential for derivatives.[18] Differentiating (A2) gives

$$\left.\frac{d\nu^{(+)}}{db}\right|_{b=b_m} = \frac{b_m + \delta}{\delta d}. \tag{A7}$$

The observed identity

$$\frac{1}{|d\nu^{(+)}/db|_{b=b_m}} = \left|\frac{\partial b}{\partial m}\right| \tag{A8}$$

suggests that upon substitution to (A1) one may expect

$$\left(\sum_{m=m_0}^{m_{\max 1}} + \sum_{m=m_0}^{m_{\max 2}}\right) \frac{1}{|d\nu^{(+)}/db|_{b=b_m}} \approx 2\sum_{m=m_0}^{m_{\max 1}} \frac{\partial b}{\partial m} \approx 2\int_0^{d/2} db = d, \tag{A9}$$

as we anticipated in Sec. IV A, but to accommodate the dependence on θ_0, we need to carry out the calculation more precisely.

Through (A3) and (A1), the differential cross section assumes the form

$$\frac{d\lambda(\theta_{\text{v.r.}},\theta_0)}{d\theta_{\text{v.r.}}} = \frac{R}{2\pi\theta_c R_c}\left(\sum_{m=0}^{m_{\max 1}} + \sum_{m=0}^{m_{\max 2}}\right) \times \frac{\delta d}{\sqrt{2\delta d(\nu^{(+)}+m) + \left(\frac{d}{2}-\delta\right)^2 - \tau^2\theta_0^2}} \approx \frac{d}{2\pi\theta_c}\sqrt{\frac{R}{R_c}} \sum_{m=0}^{R/4R_c} \frac{1}{\sqrt{m + \xi\left(\nu^{(+)}(\theta_{\text{v.r.}}),\theta_0\right)}}, \tag{A10}$$

with

$$\xi\left(\nu^{(+)}(\theta_{\text{v.r.}}),\theta_0\right) = 1 - \left\{\frac{\tau^2\theta_0^2 - \left(\frac{d}{2}-\delta\right)^2}{2\delta d} - \nu^{(+)}\right\}_{\text{f}} \equiv \left\{\frac{[b(\nu^{(+)}(\theta_{\text{v.r.}}),\theta_0)+\delta]^2}{2\delta d}\right\}_{\text{f}}. \tag{A11}$$

[18] Strictly speaking, differentiation of finite discontinuities will give δ-functional terms, but they will be imperceptible when inserted into the *denominator* of Eq. (66).

Outside the interval

$$-\frac{\pi}{2}\theta_c < \theta_{\text{v.r.}} < -\frac{\pi}{2}\theta_c\left(1 - \frac{4R_c}{R}\right), \tag{A12}$$

there are no roots to equation $\nu^{(+)}(\theta_{\text{v.r.}})$, so the differential cross section vanishes as an empty sum.

At a large upper limit, the sum in (A10) grows as $\sqrt{R/R_c}$, whereas the difference

$$\sum_{m=0}^{R/4R_c} \frac{1}{\sqrt{m+\xi}} - \sqrt{\frac{R}{R_c}} \underset{R/R_c\to\infty}{\longrightarrow} \zeta\left(\frac{1}{2},\xi\right) \tag{A13}$$

tends to a finite limit equal to a Hurwitz ζ function [whose general definition is (100)]. Thereby, we may cast (A10) as

$$\frac{d\lambda(\theta_{\text{v.r.}},\theta_0)}{d\theta_{\text{v.r.}}} \approx \frac{d}{2\pi\theta_c}\frac{R}{R_c}\left[1 + \sqrt{\frac{R_c}{R}}\zeta\left(\frac{1}{2},\xi(\theta_{\text{v.r.}},\theta_0)\right)\right]. \tag{A14}$$

Here $\sqrt{R_c/R} \ll 1$, and the unity in square brackets in (A14) corresponds to the result anticipated in (A9). But one should mind that at $\xi \to 0$, function $\zeta(\frac{1}{2},\xi)$ blows up as $\frac{1}{\sqrt{\xi}}$. So, the correction in the square brackets in (A14) cannot be regarded as everywhere small.

Now, we turn to the issue that ξ is θ_0 dependent. When θ_0 varies (at $\theta_{\text{v.r.}}$ fixed) even in a narrow interval [see (68)], ξ uniformly and repeatedly scans its definition interval from 0 to 1. Hence, the averaging over θ_0 is equivalent to the integration over ξ from 0 to 1. By virtue of the property

$$\int_0^1 d\xi\,\zeta\left(\frac{1}{2},\xi\right) \equiv 0, \tag{A15}$$

readily checkable from definition (A13) or (100), we have

$$\left\langle\frac{d\lambda}{d\theta_{\text{v.r.}}}\right\rangle_{\theta_0} = \int_0^1 d\xi \frac{d\lambda}{d\theta_{\text{v.r.}}} = \frac{Rd}{2\pi\theta_c R_c}\Theta\left(\theta_{\text{v.r.}} + \frac{\pi}{2}\theta_c\right) \times \Theta\left(-\theta_{\text{v.r.}} - \frac{\pi}{2}\theta_c\left(1 - \frac{4R_c}{R}\right)\right).$$

Thereby, we arrive at Eq. (72), without any corrections $\sim\sqrt{R_c/R}$. ■

For negatively charged particles, there arises a sum similar to that of (A1), though the dependence $\nu^{(-)}(b)$ differs a bit from $\nu^{(+)}(b)$. Nonetheless, the averaging procedure is completely analogous, the nonaveraged differential cross section equals (82) times the bracketed factor of (A14). Upon the θ_0-averaging, through (A14) again, we arrive at Eq. (82).

[1] E. N. Tsyganov, Fermilab Report No. TM-682, 1976 (unpublished); Fermilab Report No. TM-684, 1976 (unpublished); V. M. Biryukov, Yu. A. Chesnokov, and V. I. Kotov, *Crystal Channeling and its Application at High-Energy Accelerators* (Springer, Berlin, 1996); X. Artru, S. P. Fomin, N. F. Shul'ga, K. A. Ispirian, and N. K. Zhevago, Phys. Rep. **412**, 89 (2005).

[2] A. M. Taratin and S. A. Vorobiev, Nucl. Instrum. Methods B **26**, 512 (1987).

[3] Yu. M. Ivanov *et al.*, Phys. Rev. Lett. **97**, 144801 (2006); W. Scandale *et al.*, *ibid.* **98**, 154801 (2007).

[4] W. Scandale *et al.*, Phys. Lett. B **681**, 233 (2009).

[5] A. M. Taratin and W. Scandale, Nucl. Instrum. Methods B **262**, 340 (2007).

[6] M. B. H. Breese and V. M. Biryukov, Nucl. Instrum. Methods B **263**, 395 (2007); **265**, 485 (2007).

[7] W. Scandale *et al.*, Phys. Rev. Lett. **102**, 084801 (2009); W. Scandale and M. Prest, CERN Report No. CERN- SPSC-2008-014/SPSC-P-335, 2008 (unpublished).

[8] J. Lindhard, Kongel. Dan. Vidensk. Selsk., Mat.-Fys. Medd. **34**(14), 1 (1965).

[9] V. A. Maisheev, Phys. Rev. ST Accel. Beams **10**, 084701 (2007).

[10] A. M. Taratin, Phys. Part. Nucl. **29**, 437 (1998); E. Bagli, V. Guidi, and V. A. Maisheev, Phys. Rev. E **81**, 026708 (2010).

[11] V. A. Maisheev, e-print arXiv:physics/0607009v1.

[12] K. W. Ford and J. A. Wheeler, Ann. Phys. (NY) **7**, 259 (1959); N. F. Mott and H. S. W. Massey, *The Theory of Atomic Collisions* (Clarendon, Oxford, 1965); R. G. Newton, *Scattering Theory of Waves and Particles* (Springer, New York, 1982); H. M. Nussenzveig, *Diffraction Effects in Semi-Classical Scattering* (Cambridge University, Cambridge, England, 1992).

[13] G. V. Kovalev, JETP Lett. **87**, 349 (2008).

[14] F. W. J. Olver, *Asymptotics and Special Functions* (Academic, New York, 1974).

[15] W. Scandale *et al.*, Phys. Rev. Lett. **101**, 234801 (2008).

[16] W. Scandale *et al.*, Phys. Rev. A **79**, 012903 (2009).

[17] M. V. Bondarenco, Phys. Rev. A **81**, 052903 (2010).

[18] Yu. M. Ivanov *et al.*, JETP Lett. **84**, 372 (2006); V. Guidi, A. Mazzolari, D. De Salvador, and A. Carnera, J. Phys. D **42**, 182005 (2009).

[19] C. Amsler *et al.* (Particle Data Group), Phys. Lett. B **667**, 1 (2008).